

A Radio Map Approach for Reduced Pilot CSI Tracking in Massive MIMO Networks

Yuanshuai Zheng and Junting Chen

School of Science and Engineering, Shenzhen Future Network of Intelligence Institute (FNii-Shenzhen), and
Guangdong Provincial Key Laboratory of Future Networks of Intelligence
The Chinese University of Hong Kong, Shenzhen, Guangdong 518172, P. R. China

Abstract—Massive multiple-input multiple-output (MIMO) systems offer significant potential to enhance wireless communication performance, yet accurate and timely channel state information (CSI) acquisition remains a key challenge. Existing works on CSI estimation and radio map applications typically rely on stationary CSI statistics and accurate location labels. However, the CSI process can be discontinuous due to user mobility and environmental variations, and inaccurate location data can degrade the performance. By contrast, this paper studies radio-map-embedded CSI tracking and radio map construction without the assumptions of stationary CSI statistics and precise location labels. Using radio maps as the prior information, this paper develops a radio-map-embedded switching Kalman filter (SKF) framework that jointly tracks the location and the CSI with adaptive beamforming for sparse CSI observations under reduced pilots. For radio map construction without precise location labels, the location sequence and the channel covariance matrices are jointly estimated based on a Hidden Markov Model (HMM). An unbiased estimator on the channel covariance matrix is found. Numerical results on ray-traced MIMO channel datasets demonstrate that using 1 pilot in every 10 milliseconds, an average of over 97% of capacity over that of perfect CSI can be achieved, while a conventional Kalman filter (KF) can only achieve 76%. Furthermore, the proposed radio-map-embedded CSI model can reduce the localization error from 30 meters from the prior to 6 meters for radio map construction.

Index Terms—radio map, massive MIMO, channel estimation, tracking, covariance estimation

I. INTRODUCTION

MASSIVE multiple-input multiple-output (MIMO) enables spatial multiplexing, provides high beamforming gain, and supports concurrent multi-user data transmission. To realize the full potential of massive MIMO, it is essential to acquire the up-to-date channel state information (CSI), which is time-varying due to the mobility of the users and the variation of the environment. Timely CSI acquisition is challenging in massive MIMO systems because the dimension of the channel vector can be very high [1], [2].

Junting Chen is the corresponding author. The work was supported in part by the Basic Research Project No. HZQB-KCXYZ-2021067 of Hetao Shenzhen-HK S&T Cooperation Zone, by the National Science Foundation of China under Grant No. 62171398 and No. 62293482, by the Shenzhen Science and Technology Program under Grant No. JCYJ20220530143804010, No. KQTD20200909114730003, and No. KJZD20230923115104009, by Guangdong Research Projects No. 2019QN01X895, No. 2017ZT07X152, and No. 2019CX01X104, by the Shenzhen Outstanding Talents Training Fund 202002, by the Guangdong Provincial Key Laboratory of Future Networks of Intelligence (Grant No. 2022B1212010001), by the National Key R&D Program of China with grant No. 2018YFB1800800, and by the Key Area R&D Program of Guangdong Province with grant No. 2018B030338001.

Massive MIMO channel estimation and tracking generally require some prior information about the channel characteristics. If the channel covariance matrix is available, minimum mean square error (MMSE), or more generally, Bayesian approaches can be employed to constrain solutions within the subspace spanned by the covariance matrix [3], [4]. If the channel is believed to be sparse, compressive sensing techniques can be applied to obtain sparse solutions [5], [6]. Furthermore, if the channel is temporally and spatially correlated, Kalman filter (KF) approaches and autoregressive (AR) models can be leveraged to track the CSI process with reduced pilot overhead per time slot [7], [8]. Recent advancements also explore long-short term memory (LSTM)-based methods [9], [10] and some other deep learning methods, such as attention networks [11] and generative models [12].

However, if the prior information is inaccurate or varies over time, the existing methods [5]–[12] may perform poorly. For example, the channel covariance matrices may differ across locations while channel dynamics follows different models in line-of-sight (LOS) scenarios and non-line-of-sight (NLOS) scenarios. Therefore, tracking algorithms like KF may lose track of the channel when the mobile enters an NLOS region from an LOS region.

Radio maps offer a promising solution to provide prior information on channels [13]–[15]. Existing works on radio-map-assisted CSI estimation typically require location information from additional devices or via sensing. Some location-based approaches [15], [16] integrate user position information, obtained via global positioning system (GPS) or ultra-wideband (UWB) techniques, to enhance CSI prediction by exploiting spatial correlations between locations and channels. Similarly, integrated sensing and communication (ISAC) techniques [17], [18] first sense user positions and then utilize this information to assist in CSI estimation. The work [14] attempted radio-map-assisted CSI estimation without explicit location information in the estimation phase, where the radio map is a mapping from a location to a channel realization. However, such a radio map is challenging to construct without a massive amount of location-labeled data. The beam index map (BIM) proposed in [19] requires exhaustive beam sweeping at each location grid during the training process, and the beam alignment is achieved based on the accurate user position and the BIM. The work [20] focuses on constructing a channel angle map (CAM), requiring accurate information of the angle of departure (AOD) that heavily depends on user positions and

surrounding environments. Although the CAM-based method [20] can estimate both the user position and the CSI after deployment, their reliance on precise training data of AODs and user positions remains a significant limitation. Some recent attempts on channel charting developed a CSI tracking strategy without explicit user positions using deep learning techniques [21], [22], but the inherent physical mechanism is still not clear.

In this paper, we investigate the following two fundamental problems:

- *Can radio map help reduce pilots for CSI tracking?* In particular, we focus on the case where there is *no* precise location information available as an index for the CSI in the radio map. Instead, location also needs to be recovered from the pilots as an intermediate step for the CSI tracking. Thus, we aim at a joint recovery of the location and CSI using radio maps as the prior information.
- *Can we reconstruct and update a radio map from pilot sequences without precise location labels?* To construct a radio map, we need to recover precise location information from pilot sequences with possibly some side information [such as the locations of base stations \(BSs\)](#). Thus, the question is, can a radio-map-embedded CSI model help recover precise location information despite possibly NLOS?

This paper exploits the principle that while the CSI process can be discontinuous in a high-dimensional CSI space, the trajectory of the correspondingly mobile terminal has to be continuous in the three-dimensional physical world. As such, a sequence of very sparse CSI observations may suffice to discover the mobile trajectory, which leads to accurate tracking of the high-dimensional CSI with the help of radio maps. Following such a methodology, we develop a radio-map-embedded switching Kalman filter (SKF) framework that jointly tracks the location and the CSI with adaptive beamforming for sparse CSI observations under reduced pilots, where radio maps play an essential role in adjusting the operating regime of SKF. In addition, we employ a Bayesian approach for a joint estimation of the location and the channel covariance matrix from a massive amount of offline unlabeled pilot sequences for the construction of radio maps. The key theoretical contributions and numerical findings are summarized as follows:

- We propose a radio-map-embedded SKF framework for CSI tracking from a sequence of reduced pilot CSI measurements without location labels. In addition, instead of using a randomized compressive sensing approach, we develop an adaptive sensing matrix to minimize the differential entropy of the CSI.
- We develop a joint estimation on the location sequence and the channel covariance matrices from unlabeled pilot sequences using a Hidden Markov Model (HMM). An unbiased estimator on the channel covariance matrix is found with the estimation error analyzed.
- We numerically demonstrate that, in a single-user 64-antenna Multiple-Input Single-Output (MISO) system, using 1 pilot in every 10 milliseconds, an average of

over 97% of capacity over that of perfect CSI can be achieved for a user moving at 36 km/h at a 20 dB signal-to-noise ratio (SNR) under LOS, while a conventional KF can only achieve 76%. In a pure NLOS regime, the proposed radio-map-assisted approach can double the capacity from existing schemes under low to moderate SNR. For radio map construction with unlabeled pilot sequences, we demonstrate that the proposed estimation using the radio-map-embedded CSI model reduces the localization error from 30 meters from the prior to 6 meters, which is sufficient for radio map construction in our framework.

The remainder of the paper is organized as follows: Section II introduces the system model and formulates the problems of CSI tracking and radio map construction. Section III presents a radio-map-embedded SKF framework for fast CSI tracking. Section IV proposes to iteratively estimate user positions and channel covariance for radio map construction, along with the analysis of construction error. Section V provides simulations and related discussions, while Section VI concludes the paper.

Notation: Vectors and matrices are denoted by bold lower-case \mathbf{x} and bold uppercase \mathbf{X} , respectively. Scalar quantities are denoted by non-bold letters such as x . Collections are denoted by script \mathcal{X} . Probability density and mass functions are denoted by $p(\cdot)$ and $\mathbb{P}(\cdot)$, respectively. The expectation and variance operators are represented by $\mathbb{E}(\cdot)$ and $\mathbb{V}(\cdot)$, respectively. The L_2 norm is denoted by $\|\cdot\|_2$, and the Frobenius norm is denoted by $\|\cdot\|_{\text{F}}$. The conjugate transpose of a complex vector \mathbf{x} or a complex matrix \mathbf{X} is denoted by \mathbf{x}^H or \mathbf{X}^H , respectively. The trace of a matrix \mathbf{X} is denoted by $\text{tr}(\mathbf{X})$. The identity matrix is denoted by \mathbf{I} . Furthermore, we specify several key variables that will be used throughout the paper: the user position, channel state, sensing matrix, and observation at time t are denoted by \mathbf{p}_t , \mathbf{h}_t , \mathbf{A}_t , and \mathbf{y}_t , respectively. Their corresponding sequences up to time t are denoted by $\mathcal{P}_t = (\mathbf{p}_1, \mathbf{p}_2, \dots, \mathbf{p}_t)$, $\mathcal{H}_t = (\mathbf{h}_1, \mathbf{h}_2, \dots, \mathbf{h}_t)$, $\mathcal{A}_t = (\mathbf{A}_1, \mathbf{A}_2, \dots, \mathbf{A}_t)$, and $\mathcal{Y}_t = (\mathbf{y}_1, \mathbf{y}_2, \dots, \mathbf{y}_t)$, with their realizations when $t = T$ denoted by $\mathcal{P}_T = (\mathbf{p}_1, \mathbf{p}_2, \dots, \mathbf{p}_T)$, $\mathcal{H}_T = (\mathbf{h}_1, \mathbf{h}_2, \dots, \mathbf{h}_T)$, $\mathcal{A}_T = (\mathbf{A}_1, \mathbf{A}_2, \dots, \mathbf{A}_T)$, and $\mathcal{Y}_T = (\mathbf{y}_1, \mathbf{y}_2, \dots, \mathbf{y}_T)$, respectively.

II. SYSTEM MODEL

A. Network Topology, Channel Model, and Radio Map Model

Consider a MIMO network with Q BSs and one mobile user, where each BS is equipped with N_t antennas and the user has a single antenna. To ease the elaboration, we simply illustrate the case of $Q = 1$ because, for $Q > 1$, we can simply stack variables and increase the dimension of the system states, where the form of the formulas for the multi-BS case is similar.

Suppose that the environment is quasi-static, where the majority of the scatters are static and only a small portion of scatters are time-varying. The static scatters may correspond to the ground and buildings, and the time-varying scatters may correspond to the vehicles and pedestrians. We are interested in the scenarios where the MIMO BSs are placed on the rooftop or tower, where there are few moving scatters near the BSs.

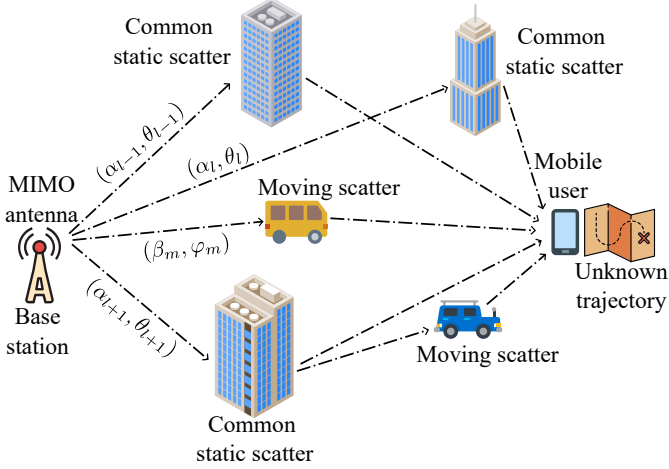


Figure 1. Illustration of the channel in a quasi-static environment, where the majority of the scatterers are static and a small portion of scatterers are time-varying, and adjacent mobile locations may share common static scatterers.

The propagation between the BS and the user located at \mathbf{p} can be modeled as signal aggregation from the set of propagation paths $\mathcal{N}_s(\mathbf{p})$ via static scatterers and from the paths $\mathcal{N}_m(\mathbf{p})$ via moving scatterers. As illustrated in Fig. 1, a geometric narrow-band multipath MIMO channel can be modeled as [23]

$$\mathbf{h}(\mathbf{p}) = \sum_{l \in \mathcal{N}_s(\mathbf{p})} a_l(\mathbf{p}) \boldsymbol{\alpha}(\theta_l(\mathbf{p})) + \sum_{m \in \mathcal{N}_m(\mathbf{p})} \beta_m \boldsymbol{\alpha}(\varphi_m), \quad (1)$$

where the coefficients a_l and β_m denote the complex path gains, $\theta_l(\mathbf{p})$ and φ_m denote the AOD at the BS, and $\boldsymbol{\alpha}(\theta)$ denotes the steering vector at θ according to the antenna geometry of the BS. The statistics of the coefficients $a_l(\mathbf{p})$ from the static scatterers depend on the user location \mathbf{p} , whereas the coefficients β_m and the AOD φ_m from the moving scatterers are assumed to be independent of \mathbf{p} .

Based on (1), the multipath channel can be written as

$$\mathbf{h}(\mathbf{p}) \triangleq \mathbf{h}^s(\mathbf{p}) + \mathbf{h}^e, \quad (2)$$

where $\mathbf{h}^s(\mathbf{p}) \triangleq \sum_{l \in \mathcal{N}_s(\mathbf{p})} a_l(\mathbf{p}) \boldsymbol{\alpha}(\theta_l(\mathbf{p}))$ is the channel due to static scattering for user location \mathbf{p} , and $\mathbf{h}^e \triangleq \sum_{m \in \mathcal{N}_m(\mathbf{p})} \beta_m \boldsymbol{\alpha}(\varphi_m)$ is the channel due to the moving scatterers. It is assumed that both $\mathbf{h}^s(\mathbf{p})$ and \mathbf{h}^e have zero mean and they are independent.

Consider a discrete location model, where the area of interest is partitioned into equally spaced grids. The user is located at one of the grid points $\mathbf{x} \in \mathcal{X}$, where \mathcal{X} is a collection of all the grid locations. We define the radio map as a collection of the discretized location $\mathbf{x} \in \mathcal{X}$ and the covariance matrix $\mathbf{C}(\mathbf{x})$ pairs, *i.e.*, $\mathcal{M} = \{(\mathbf{x}, \mathbf{C}(\mathbf{x})) : \mathbf{x} \in \mathcal{X}\}$, where $\mathbf{C}(\mathbf{x}) \triangleq \mathbb{E}\{\mathbf{h}\mathbf{h}^H\}$, in which the expectation is taken over the distribution of the positions \mathbf{p} within the grid cell with a center location $\mathbf{x} \in \mathcal{X}$ and the small-scale fading of the channel. We assume that $\mathbf{h}^s(\mathbf{p})$ is spatially correlated for all the positions \mathbf{p} in the same grid cell and $\mathbb{E}\{\mathbf{h}^e(\mathbf{h}^e)^H\} = \sigma_h^2 \mathbf{I}$, where σ_h^2 is much smaller than the mean energy of $\mathbf{h}^s(\mathbf{p})$. Hence, the distribution of the channel $f_h(\mathbf{h})$ given the location \mathbf{x} is fully captured by the covariance matrix $\mathbf{C}(\mathbf{x})$ and the parameter σ_h^2 .

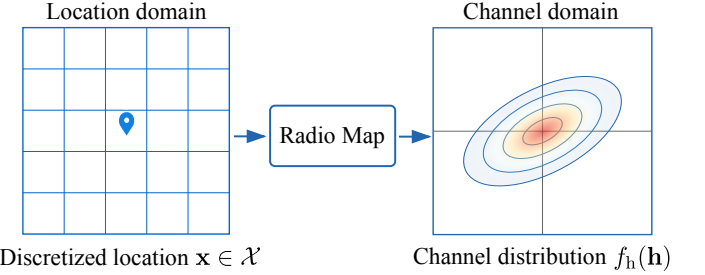


Figure 2. Illustration of the radio map. The area of interest is partitioned into grid cells. The radio map is a mapping from a grid cell to a channel distribution $f_h(\mathbf{h}|\mathbf{x}_i)$, where \mathbf{x}_i is a discretized location representing the i th grid cell.

With such a discretized model, we now consider that \mathbf{p} takes a discrete position from \mathcal{X} in the rest of the paper.

B. System Dynamics

Consider that the mobile user moves along a trajectory $\mathcal{P}_t = (\mathbf{p}_1, \mathbf{p}_2, \dots, \mathbf{p}_t)$ that can be described by a Markov chain with known transition probability $\mathbb{P}(\mathbf{p}_t|\mathbf{p}_{t-1})$. Such prior information can be obtained empirically from prior measurements. For example, one can assume a uniform prior $\mathbb{P}(\mathbf{p}_t = \mathbf{x}_j|\mathbf{p}_{t-1} = \mathbf{x}_i)$ for a reasonable range of speed of a vehicle. Alternatively, the transition probability $\mathbb{P}(\mathbf{p}_t = \mathbf{x}_i|\mathbf{p}_{t-1} = \mathbf{x}_j)$ can be specified using a truncated Gauss-Markov model [24] over the coordinates of the i th and j th grid points for $\mathbf{x}_i, \mathbf{x}_j \in \mathcal{X}$,

$$\mathbb{P}(\mathbf{p}_t = \mathbf{x}_i|\mathbf{p}_{t-1} = \mathbf{x}_j) \propto \begin{cases} \exp(-\|\mathbf{x}_i - (\mathbf{x}_j + \delta_t \bar{\mathbf{v}})\|_2^2) & \text{if } \|\mathbf{x}_i - \mathbf{x}_j\|_2^2 \leq \eta \delta_t \\ 0 & \text{otherwise,} \end{cases} \quad (3)$$

where η determines the maximum possible speed, $\bar{\mathbf{v}}$ is the average speed, and δ_t is the time slot duration.

A radio-map-embedded first-order AR model [8] for the dynamic of the channel \mathbf{h}_t is considered as

$$\mathbf{h}_t = \gamma \mathbf{h}_{t-1} + \sqrt{1 - \gamma^2} \mathbf{u}_t, \quad (4)$$

where $\mathbf{u}_t \sim \mathcal{CN}(0, \mathbf{C}(\mathbf{p}_t))$, and $\gamma \in [0, 1]$ determines the level of temporal correlation between the current channel \mathbf{h}_t and the previous channel \mathbf{h}_{t-1} . Additionally, the scaling factor $\sqrt{1 - \gamma^2}$ ensures that the disturbance term \mathbf{u}_t maintains the appropriate variance to preserve the statistical properties of the channel model. It is worth highlighting that the statistics of the disturbance \mathbf{u}_t depend on the user position \mathbf{p}_t due to the geographic-specific spatial correlation of the channel, and the statistics $\mathbf{C}(\mathbf{p}_t)$ are captured by the radio map. It can be verified that the stationary distribution of \mathbf{h}_t follows $\mathcal{CN}(0, \mathbf{C}(\mathbf{p}_t))$ which is consistent with our radio map model.

At each time slot, the channel is probed using a small set of sensing vectors, and the observation is given by

$$\mathbf{y}_t = \mathbf{A}_t \mathbf{h}_t + \mathbf{n}_t, \quad (5)$$

where $\mathbf{A}_t \in \mathbb{C}^{M \times N_t}$ is a semi-unitary sparse combining matrix satisfying $\mathbf{A}_t \mathbf{A}_t^H = \mathbf{I}$ with $M \ll N_t$, and \mathbf{n}_t represents

the measurement noise. The noise is assumed to follow a zero-mean complex Gaussian distribution, *i.e.*, $\mathbf{n}_t \sim \mathcal{CN}(\mathbf{0}, \sigma_n^2 \mathbf{I})$, where σ_n^2 is the noise variance.

The observation model (5) provides a unified representation for both uplink and downlink implementations. In the uplink case, the BS receives the signal $\mathbf{y}_t = \mathbf{A}_t \mathbf{h}_t s + \mathbf{n}_t \in \mathbb{C}^M$ through the beamforming matrix \mathbf{A}_t , where the rows serve as combining vectors. The parameter M may not be greater than the number of available radio-frequency (RF) chains at the BS. We can simply take $s = 1$ without loss of generality (w.l.o.g.) to yield the observation model (5). In the downlink case, the BS transmits a beamformed pilot $\mathbf{a}_t^* s$ (with s again assumed to be 1) where \mathbf{a}_t^* is the conjugate of \mathbf{a}_t , and the user receives the signal as $y_t = \mathbf{h}_t^T \mathbf{a}_t^* s + n_t$, where y_t and n_t denote the scalar observation and noise, respectively. Then, the user may feed back the estimated channel or simply the received scalar y_t to the BS. The matrix \mathbf{A}_t in this case comprises M beamforming vectors, with each row of \mathbf{A}_t given by the conjugate transpose of a beamforming vector \mathbf{a}_t . Thus, the model in (5) also captures the downlink scenario in a unified form.

C. The CSI Tracking Problem

Denote $\mathcal{Y}_t = (\mathbf{y}_1, \mathbf{y}_2, \dots, \mathbf{y}_t)$ as the sequence of sparse observations along the trajectory $\mathcal{P}_t = (\mathbf{p}_1, \mathbf{p}_2, \dots, \mathbf{p}_t)$ based on sensing matrices $\mathcal{A}_t = (\mathbf{A}_1, \mathbf{A}_2, \dots, \mathbf{A}_t)$, where the CSI sequence is denoted as $\mathcal{H}_t = (\mathbf{h}_1, \mathbf{h}_2, \dots, \mathbf{h}_t)$. The goal of this paper is to track the CSI \mathcal{H}_t based on the sequence of sparse observations \mathcal{Y}_t . In particular, we propose to recover the trajectory \mathcal{P}_t as an intermediate step to assist the CSI tracking via the radio map $\mathcal{M} = \{(\mathbf{x}, \mathbf{C}(\mathbf{x})) : \mathbf{x} \in \mathcal{X}\}$. In turn, we also need to construct or update the radio map \mathcal{M} based on \mathcal{Y}_t and \mathcal{P}_t .

1) *Radio-Map-Embedded CSI Tracking*: Most existing radio-map-embedded CSI estimation or beam-tracking approaches require location information [15], [25], or an estimate of the location based on a one-shot CSI measurement \mathbf{y}_t [20]. When a sequence of measurement \mathcal{Y}_t is available, one may estimate the entire CSI sequence \mathcal{H}_t by maximizing the joint probability $p(\mathcal{Y}_t, \mathcal{H}_t)$ or by minimizing the mean squared error (MSE) for \mathcal{H}_t based on the joint distribution $p(\mathcal{Y}_t, \mathcal{H}_t)$. A classical algorithm is KF [7], [8], but it requires the channel to be temporally correlated with smooth statistics. Specifically, a conventional KF requires the covariance matrix $\mathbf{C}(\mathbf{p}_t)$ in (4) to be continuous in space, without jumps. However, in a dense urban scenario, the temporal and spatial correlation of the channel \mathbf{h}_t can be destroyed by sudden signal blockage due to mobility, and therefore, the process of the covariance matrix $\mathbf{C}(\mathbf{p}_t)$ can be *discontinuous* and with jumps in space.

Therefore, we propose to develop a new CSI tracking strategy based on the spatial correlation of the hidden trajectory \mathcal{P}_t , which has to be *continuous* due to Newton's law. *However*, \mathcal{P}_t is not observed but treated as a latent variable to be estimated. Once estimated, one can track the CSI using the prior information from the radio map \mathcal{M} , without assuming any correlation between $\mathbf{C}(\mathbf{p}_t)$ and $\mathbf{C}(\mathbf{p}_{t-1})$. Mathematically,

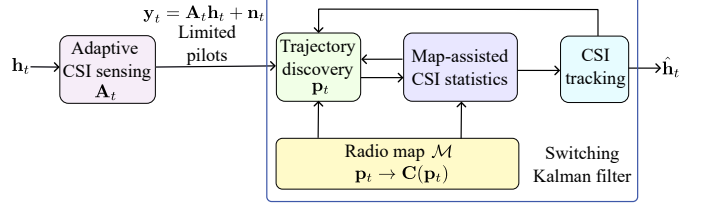


Figure 3. Diagram of the radio-map-embedded CSI tracking framework.

when a maximum log-likelihood criterion is considered, the CSI tracking problem can be formulated as follows

$$\begin{aligned} \mathcal{P}_1 : \quad & \underset{\mathcal{H}_T, \mathcal{P}_T, \mathcal{A}_T}{\text{maximize}} \quad \log p(\mathcal{Y}_T, \mathcal{H}_T, \mathcal{P}_T; \mathcal{A}_T, \mathcal{M}) \\ & \text{subject to} \quad \mathbf{p}_t \in \mathcal{X}, \quad t = 1, 2, \dots, T \end{aligned}$$

where $p(\mathcal{Y}_T, \mathcal{H}_T, \mathcal{P}_T; \mathcal{A}_T, \mathcal{M})$ denotes the joint probability of $\mathcal{Y}_T = (\mathbf{y}_1, \mathbf{y}_2, \dots, \mathbf{y}_T)$, $\mathcal{H}_T = (\mathbf{h}_1, \mathbf{h}_2, \dots, \mathbf{h}_T)$, and $\mathcal{P}_T = (\mathbf{p}_1, \mathbf{p}_2, \dots, \mathbf{p}_T)$, given the sequence of sensing matrices $\mathcal{A}_T = (\mathbf{A}_1, \mathbf{A}_2, \dots, \mathbf{A}_T)$ and the covariance matrices $\mathbf{C}(\mathbf{p}_t)$ from the radio map \mathcal{M} .

2) *Radio Map Construction*: To construct the radio map \mathcal{M} , the anchor information is needed, because there is no additional geographic information in \mathcal{P}_1 except \mathcal{M} . Denote Θ as a collection of the BS locations. Denote $f(\mathcal{Y}_T, \mathcal{P}_T; \Theta)$ as the value function to measure the likelihood of how the sequence of observations \mathcal{Y}_T matches with the trajectory \mathcal{P}_T given the network topology Θ , such as the BS locations. Given the entire history of measurements, a topology-regularized maximum log-likelihood problem for radio map construction is formulated as follows

$$\begin{aligned} \mathcal{P}_2 : \quad & \underset{\mathcal{H}_T, \mathcal{P}_T, \mathcal{M}}{\text{maximize}} \quad \log p(\mathcal{Y}_T, \mathcal{H}_T, \mathcal{P}_T; \mathcal{M}) \\ & \quad - \mu f(\mathcal{Y}_T, \mathcal{P}_T; \Theta) \\ & \text{subject to} \quad \mathbf{p}_t \in \mathcal{X}, \quad t = 1, 2, \dots, T \end{aligned}$$

where $\mu > 0$ serves as a regularization parameter. The radio map variable \mathcal{M} in \mathcal{P}_2 is constructed via estimating the covariance matrices $\mathbf{C}(\mathbf{x})$ for all $\mathbf{x} \in \mathcal{X}$.

III. RADIO-MAP-EMBEDDED CSI TRACKING WITH A SWITCHING KALMAN FILTER FRAMEWORK

In this section, we are interested in a tracking approach to solve problem \mathcal{P}_1 . Specifically, we develop a radio-map-embedded SKF framework for CSI tracking as shown in Fig. 3. First, given a sequence of sensing matrices \mathcal{A}_t , the position \mathbf{p}_t and the CSI \mathbf{h}_t are jointly estimated and tracked, where an SKF is applied to track \mathbf{h}_t with switching dynamics based on the distribution of the position \mathbf{p}_t and the radio map \mathcal{M} , and in turn, the position \mathbf{p}_t is estimated and tracked based on the estimate of \mathbf{h}_t . Second, the sensing matrix \mathbf{A}_t is dynamically adjusted by minimizing the differential entropy of the channel.

As the radio map \mathcal{M} is given in this section, to simplify the notation, we omit the symbols \mathcal{A}_T and \mathcal{M} in the joint probability $p(\mathcal{Y}_T, \mathcal{H}_T, \mathcal{P}_T; \mathcal{A}_T, \mathcal{M})$, wherever it does not affect the clarity from the context.

A. Problem Reformulation

Using Bayes' theorem, the joint probability $p(\mathcal{Y}_T, \mathcal{H}_T, \mathcal{P}_T)$ is explicitly expressed in the following proposition.

Proposition 1 (Factorization of $p(\mathcal{Y}_T, \mathcal{H}_T, \mathcal{P}_T)$). *The joint probability $p(\mathcal{Y}_T, \mathcal{H}_T, \mathcal{P}_T)$ can be factorized as*

$$p(\mathcal{Y}_T, \mathcal{H}_T, \mathcal{P}_T) = \prod_{t=1}^T p(\mathbf{y}_t | \mathbf{h}_t) \prod_{t=2}^T p(\mathbf{h}_t | \mathbf{h}_{t-1}, \mathbf{p}_t) \\ \times p(\mathbf{h}_1) \times \prod_{t=2}^T \mathbb{P}(\mathbf{p}_t | \mathbf{p}_{t-1}) \mathbb{P}(\mathbf{p}_1). \quad (6)$$

Proof. See Appendix A. \square

With the factorization (6) and given the sensing matrices \mathcal{A}_T , problem \mathcal{P}_1 becomes

$$\mathcal{P}'_1 : \underset{\mathcal{H}_T, \mathcal{P}_T}{\text{maximize}} \quad \sum_{t=1}^T \log p(\mathbf{y}_t | \mathbf{h}_t) + \log p(\mathbf{h}_1) \\ + \sum_{t=2}^T \log p(\mathbf{h}_t | \mathbf{h}_{t-1}, \mathbf{p}_t) \\ + \log \mathbb{P}(\mathbf{p}_1) + \sum_{t=2}^T \log \mathbb{P}(\mathbf{p}_t | \mathbf{p}_{t-1}) \\ \text{subject to} \quad \mathbf{p}_t \in \mathcal{X}, \quad t = 1, 2, \dots, T.$$

B. Radio-Map-Embedded Switching Kalman Filtering

Here, we develop an SKF approach to jointly track the positions and the CSI. We first find the distribution of the position \mathbf{p}_t given the measurements up to time t and the trajectory up to time $t-1$. Then, with the radio map \mathcal{M} and the conditional distribution of \mathbf{p}_t , the CSI \mathbf{h}_t is recursively tracked leveraging an SKF. Finally, the position \mathbf{p}_t is estimated based on the maximum likelihood criterion.

1) *Distribution of the Position:* Let $\pi_t(\mathbf{p}_t) \triangleq p(\mathbf{p}_t | \mathcal{Y}_t, \mathcal{P}_{t-1})$ be the distribution of the position at time t given the measurements up to time t and the trajectory up to time $t-1$. Using Bayes' theorem, for $t = 2, 3, \dots, T$, $\pi_t(\mathbf{p}_t)$ is derived as

$$\pi_t(\mathbf{p}_t) = p(\mathbf{p}_t | \mathcal{Y}_t, \mathcal{P}_{t-1}) \\ = \frac{p(\mathcal{Y}_t, \mathcal{P}_{t-1}, \mathbf{p}_t)}{p(\mathcal{Y}_t, \mathcal{P}_{t-1})} \quad (7)$$

$$= \frac{p(\mathcal{Y}_t, \mathcal{P}_t)}{p(\mathcal{Y}_t, \mathcal{P}_{t-1})} \quad (8)$$

$$= \frac{p(\mathbf{y}_t | \mathcal{Y}_{t-1}, \mathcal{P}_t) p(\mathbf{p}_t | \mathcal{Y}_{t-1}, \mathcal{P}_{t-1}) p(\mathcal{Y}_{t-1}, \mathcal{P}_{t-1})}{p(\mathbf{y}_t | \mathcal{Y}_{t-1}, \mathcal{P}_{t-1}) p(\mathcal{Y}_{t-1}, \mathcal{P}_{t-1})} \quad (9)$$

$$= \frac{p(\mathbf{y}_t | \mathbf{p}_t) \mathbb{P}(\mathbf{p}_t | \mathbf{p}_{t-1})}{\sum_{\mathbf{x} \in \mathcal{X}} p(\mathbf{y}_t | \mathbf{x}) \mathbb{P}(\mathbf{x} | \mathbf{p}_{t-1})}, \quad (10)$$

where equation (7) follows from the definition of conditional probability, equation (8) uses the identity that $\mathcal{P}_t = (\mathbf{p}_1, \mathbf{p}_2, \dots, \mathbf{p}_t)$ and $\mathcal{P}_{t-1} = (\mathbf{p}_1, \mathbf{p}_2, \dots, \mathbf{p}_{t-1})$, equation (9) holds since both $p(\mathcal{Y}_t, \mathcal{P}_t)$ and $p(\mathcal{Y}_t, \mathcal{P}_{t-1})$ can be derived in a similar manner to (42), and equation (10) holds because \mathbf{y}_t depends on \mathbf{p}_t which depends on \mathbf{p}_{t-1} . The conditional

probability $p(\mathbf{y}_t | \mathbf{p}_t)$ can be derived based on the observation model (5) and the channel distribution $\mathbf{h}_t | \mathbf{p}_t \sim \mathcal{CN}(0, \mathbf{C}(\mathbf{p}_t))$ indicated in (4) as

$$p(\mathbf{y}_t | \mathbf{p}_t) = \frac{\exp(-\frac{1}{2} \mathbf{y}_t^H (\mathbf{A}_t \mathbf{C}(\mathbf{p}_t) \mathbf{A}_t^H + \sigma_n^2 \mathbf{I})^{-1} \mathbf{y}_t)}{\sqrt{(2\pi)^M |\mathbf{A}_t \mathbf{C}(\mathbf{p}_t) \mathbf{A}_t^H + \sigma_n^2 \mathbf{I}|}}. \quad (11)$$

2) *Radio-Map-Embedded CSI Tracking:* First, we derive a CSI prediction and its corresponding error covariance at time t based on the observations \mathcal{Y}_{t-1} up to time $t-1$.

Define $\hat{\mathbf{h}}_{t-1} \triangleq \mathbb{E}\{\mathbf{h}_{t-1} | \mathcal{Y}_{t-1}\}$ as the Bayesian estimator of the CSI \mathbf{h}_{t-1} based on the observations \mathcal{Y}_{t-1} up to time $t-1$. Define $\hat{\mathbf{h}}_{t|t-1} \triangleq \mathbb{E}\{\mathbf{h}_t | \hat{\mathbf{h}}_{t-1}\}$ as a prediction of the CSI \mathbf{h}_t based on $\hat{\mathbf{h}}_{t-1}$. Using the CSI dynamic model (4), we have

$$\hat{\mathbf{h}}_{t|t-1} = \mathbb{E}\{\mathbf{h}_t | \hat{\mathbf{h}}_{t-1}\} = \gamma \hat{\mathbf{h}}_{t-1}. \quad (12)$$

Define $\mathbf{e}_{t|t-1} \triangleq \mathbf{h}_t - \hat{\mathbf{h}}_{t|t-1}$ as the channel prediction error of \mathbf{h}_t based on the observations \mathcal{Y}_{t-1} up to time $t-1$. Substituting (12) into $\mathbf{e}_{t|t-1}$, we can obtain

$$\mathbf{e}_{t|t-1} \triangleq \mathbf{h}_t - \hat{\mathbf{h}}_{t|t-1} \\ = \gamma \mathbf{h}_{t-1} + \sqrt{1 - \gamma^2} \mathbf{u}_t - \gamma \hat{\mathbf{h}}_{t-1} \\ = \gamma \mathbf{e}_{t-1} + \sqrt{1 - \gamma^2} \mathbf{u}_t, \quad (13)$$

where \mathbf{e}_{t-1} is the channel estimation error generated from the Bayesian estimator $\hat{\mathbf{h}}_{t-1}$, i.e., $\mathbf{e}_{t-1} \triangleq \mathbf{h}_{t-1} - \hat{\mathbf{h}}_{t-1}$.

Following the channel prediction error $\mathbf{e}_{t|t-1}$ in (13), the error covariance of $\mathbf{e}_{t|t-1}$ is derived as

$$\mathbf{Q}_{t|t-1} \triangleq \mathbb{E}\{\mathbf{e}_{t|t-1} \mathbf{e}_{t|t-1}^H\} \\ = \gamma^2 \mathbb{E}\{\mathbf{e}_{t-1} \mathbf{e}_{t-1}^H\} + (1 - \gamma^2) \mathbb{E}\{\mathbf{u}_t \mathbf{u}_t^H | \mathbf{p}_{t-1}\} \\ = \gamma^2 \mathbf{Q}_{t-1} + (1 - \gamma^2) \mathbb{E}\{\mathbf{u}_t \mathbf{u}_t^H | \mathbf{p}_{t-1}\}, \quad (14)$$

where $\mathbf{Q}_{t-1} \triangleq \mathbb{E}\{\mathbf{e}_{t-1} \mathbf{e}_{t-1}^H\}$ is the error covariance of \mathbf{e}_{t-1} , and the term $\mathbb{E}\{\mathbf{u}_t \mathbf{u}_t^H | \mathbf{p}_{t-1}\}$ can be computed based on the distribution of the position \mathbf{p}_t given \mathbf{p}_{t-1} in (10) and the radio map \mathcal{M} as follows

$$\mathbb{E}\{\mathbf{u}_t \mathbf{u}_t^H | \mathbf{p}_{t-1}\} = \mathbb{E}_{\mathbf{p}_t \in \mathcal{X}} \{\mathbb{E}\{\mathbf{u}_t \mathbf{u}_t^H | \mathbf{p}_t\} | \mathbf{p}_{t-1}\} \\ = \sum_{\mathbf{p}_t \in \mathcal{X}} \pi_t(\mathbf{p}_t) \times \mathbf{C}(\mathbf{p}_t), \quad (15)$$

where recall from (4) that $\mathbf{u}_t | \mathbf{p}_t \sim \mathcal{CN}(0, \mathbf{C}(\mathbf{p}_t))$ implying $\mathbb{E}\{\mathbf{u}_t \mathbf{u}_t^H | \mathbf{p}_t\} = \mathbf{C}(\mathbf{p}_t)$, and $\pi_t(\mathbf{p}_t)$ captures the location distribution at time t based on observations \mathcal{Y}_t up to time t and the user trajectory \mathcal{P}_{t-1} up to time $t-1$. It is observed that the radio map \mathcal{M} plays a critical role in constructing the distribution of the hidden position variable \mathbf{p}_t and the error covariance $\mathbf{Q}_{t|t-1}$ for the channel prediction.

Second, an update equation for the Bayesian estimator $\hat{\mathbf{h}}_t \triangleq \mathbb{E}\{\mathbf{h}_t | \mathcal{Y}_t\}$ based on the observations \mathcal{Y}_t up to time t can be formulated as [26]

$$\hat{\mathbf{h}}_t = \hat{\mathbf{h}}_{t|t-1} + \mathbf{K}_t (\mathbf{y}_t - \mathbf{A}_t \hat{\mathbf{h}}_{t|t-1}), \quad (16)$$

where \mathbf{K}_t is a coefficient of the measurement residual $\mathbf{y}_t - \mathbf{A}_t \hat{\mathbf{h}}_{t|t-1}$. The optimal coefficient \mathbf{K}_t that minimizes the mean squared error of the estimator $\hat{\mathbf{h}}_t$ is given by [26]

$$\mathbf{K}_t = \mathbf{Q}_{t|t-1} \mathbf{A}_t^H (\mathbf{A}_t \mathbf{Q}_{t|t-1} \mathbf{A}_t^H + \sigma_n^2 \mathbf{I})^{-1}. \quad (17)$$

It is observed from (17) that the optimal \mathbf{K}_t relies on the error covariance $\mathbf{Q}_{t|t-1}$, which is partially determined by the channel spatial statistics $\mathbb{E}\{\mathbf{u}_t \mathbf{u}_t^H | \mathbf{p}_{t-1}\}$, and thus the radio map \mathcal{M} .

Based on (16) and (17), the covariance of the estimation error $\mathbf{e}_t \triangleq \mathbf{h}_t - \hat{\mathbf{h}}_t$ can be derived as

$$\begin{aligned} \mathbf{Q}_t &\triangleq \mathbb{E}\{(\mathbf{h}_t - \hat{\mathbf{h}}_t)(\mathbf{h}_t - \hat{\mathbf{h}}_t)^H\} \\ &= (\mathbf{I} - \mathbf{K}_t \mathbf{A}_t) \mathbf{Q}_{t|t-1} (\mathbf{I} - \mathbf{K}_t \mathbf{A}_t)^H + \mathbf{K}_t \mathbf{K}_t^H / \sigma_n^2 \\ &= (\mathbf{I} - \mathbf{K}_t \mathbf{A}_t) \mathbf{Q}_{t|t-1} \end{aligned} \quad (18)$$

which completes the recursive filter.

3) *User Position Tracking*: Based on the observation sequence \mathcal{Y}_t , the CSI sequence \mathcal{H}_t up to time t , and the user trajectory \mathcal{P}_{t-1} , the user position at time $t = 2, 3, \dots, T$ can be tracked by maximizing the conditional probability $\bar{\pi}_t(\mathbf{p}_t) \triangleq p(\mathbf{p}_t | \mathcal{Y}_t, \mathcal{H}_t, \mathcal{P}_{t-1})$. Similar to (10), $\bar{\pi}_t(\mathbf{p}_t)$ can be derived as

$$\begin{aligned} \bar{\pi}_t(\mathbf{p}_t) &\triangleq p(\mathbf{p}_t | \mathcal{Y}_t, \mathcal{H}_t, \mathcal{P}_{t-1}) \\ &= \frac{p(\mathcal{Y}_t, \mathcal{H}_t, \mathcal{P}_{t-1}, \mathbf{p}_t)}{p(\mathcal{Y}_t, \mathcal{H}_t, \mathcal{P}_{t-1})} \end{aligned} \quad (19)$$

$$= \frac{p(\mathcal{Y}_t, \mathcal{H}_t, \mathcal{P}_t)}{p(\mathcal{Y}_t, \mathcal{H}_t, \mathcal{P}_{t-1})} \quad (20)$$

$$= \frac{p(\mathbf{h}_t | \mathbf{h}_{t-1}, \mathbf{p}_t) \mathbb{P}(\mathbf{p}_t | \mathbf{p}_{t-1})}{\sum_{\mathbf{x} \in \mathcal{X}} p(\mathbf{h}_t | \mathbf{h}_{t-1}, \mathbf{x}) \mathbb{P}(\mathbf{x} | \mathbf{p}_{t-1})}, \quad (21)$$

where equation (19) follows from the definition of conditional probability, equation (20) uses the identity that $\mathcal{P}_t = (\mathbf{p}_1, \mathbf{p}_2, \dots, \mathbf{p}_t)$ and $\mathcal{P}_{t-1} = (\mathbf{p}_1, \mathbf{p}_2, \dots, \mathbf{p}_{t-1})$, and equation (21) holds because the joint distribution $p(\mathcal{Y}_t, \mathcal{H}_t, \mathcal{P}_t)$ is given in (46), and $p(\mathcal{Y}_t, \mathcal{H}_t, \mathcal{P}_{t-1})$ is obtained by marginalizing $p(\mathcal{Y}_t, \mathcal{H}_t, \mathcal{P}_t)$ over \mathbf{p}_t . In addition, the conditional distribution $\mathbf{h}_t | \mathbf{h}_{t-1}, \mathbf{p}_t \sim \mathcal{CN}(\gamma \mathbf{h}_{t-1}, (1 - \gamma^2) \mathbf{C}(\mathbf{p}_t))$ follows from (4).

Based on (21), the user position at time $t = 2, 3, \dots, T$ can be obtained as

$$\begin{aligned} \hat{\mathbf{p}}_t &= \operatorname{argmax}_{\mathbf{p}_t \in \mathcal{X}} p(\mathbf{h}_t | \mathbf{h}_{t-1}, \mathbf{p}_t) \mathbb{P}(\mathbf{p}_t | \mathbf{p}_{t-1}) \\ &= \operatorname{argmax}_{\mathbf{p}_t \in \mathcal{X}} \frac{\exp(-\frac{1}{2} \mathbf{\Delta}_t^H ((1 - \gamma^2) \mathbf{C}(\mathbf{p}_t))^{-1} \mathbf{\Delta}_t)}{\sqrt{(2\pi(1 - \gamma^2))^N | \mathbf{C}(\mathbf{p}_t) |}} \mathbb{P}(\mathbf{p}_t | \mathbf{p}_{t-1}) \end{aligned} \quad (22)$$

where $\mathbf{\Delta}_t \triangleq \mathbf{h}_t - \gamma \mathbf{h}_{t-1}$.

The overall algorithm of the radio-map-embedded SKF is summarized in Algorithm 1. The complexity of Algorithm 1 is analyzed as follows. At each time step, the computational complexity for CSI tracking is $O(|\mathcal{X}|N_t^2 + N_t^2 M + M^3 + N_t^3)$. Specifically the term $O(|\mathcal{X}|N_t^2)$ arises from computing the spatial statistics of CSI in (15), $O(N_t^2 M + M^3)$ results from matrix operations in CSI estimation, such as computing $\mathbf{Q}_{t|t-1} \mathbf{A}_t^H$ in (17), and $O(N_t^3)$ is due to the matrix inversion involved in user localization in (22).

C. Entropy-based Sensing Matrix Adaptation

As can be seen in (16), the update of the channel estimator $\hat{\mathbf{h}}_t$ from $\hat{\mathbf{h}}_{t|t-1}$ relies on the observation \mathbf{y}_t which is influenced by the sensing matrix \mathbf{A}_t . When no prior information is

Algorithm 1 Radio-Map-Embedded SKF for Online CSI Tracking

Input: Radio maps \mathcal{M} , noise variance σ_n^2 , and an initialized position $\hat{\mathbf{p}}_1$ (such as from a uniform prior).

- 1) At time $t = 1$, randomly generate \mathbf{A}_1 to observe \mathbf{y}_1 . Initialize $\hat{\mathbf{h}}_1 \sim \mathcal{CN}(0, \mathbf{C}(\hat{\mathbf{p}}_1))$ and $\mathbf{Q}_1 = (1 - \gamma^2) \sum_{\mathbf{p}_1 \in \mathcal{X}} \pi_1(\mathbf{p}_1) \times \mathbf{C}(\mathbf{p}_1)$, where $\pi_1(\mathbf{p}_1) = p(\mathbf{p}_1 | \mathbf{y}_1)$.
- 2) For each $t > 1$:
 - a) Channel prediction based on observations \mathcal{Y}_{t-1} :
 - i) $\hat{\mathbf{h}}_{t|t-1} = \gamma \hat{\mathbf{h}}_{t-1}$.
 - ii) $\mathbf{Q}_{t|t-1} = \gamma^2 \mathbf{Q}_{t-1} + (1 - \gamma^2) \sum_{\mathbf{p}_t \in \mathcal{X}} \mathbb{P}(\mathbf{p}_t | \mathbf{p}_{t-1}) = \hat{\mathbf{p}}_{t-1} \times \mathbf{C}(\mathbf{p}_t)$, where $\mathbb{P}(\mathbf{p}_t | \mathbf{p}_{t-1}) = \hat{\mathbf{p}}_{t-1}$ is given in (3) and $\mathbf{C}(\mathbf{p}_t)$ is embedded in the radio map \mathcal{M} .
 - b) Design \mathbf{A}_t using (32) based on $\mathbf{Q}_{t|t-1}$ and perform channel sensing using \mathbf{A}_t to obtain \mathbf{y}_t .
 - c) Refine $\mathbf{Q}_{t|t-1}$ as $\mathbf{Q}_{t|t-1} = \gamma^2 \mathbf{Q}_{t-1} + (1 - \gamma^2) \mathbb{E}\{\mathbf{u}_t \mathbf{u}_t^H | \mathbf{p}_{t-1} = \hat{\mathbf{p}}_{t-1}\}$, where $\mathbb{E}\{\mathbf{u}_t \mathbf{u}_t^H | \mathbf{p}_{t-1} = \hat{\mathbf{p}}_{t-1}\} = \sum_{\mathbf{p}_t \in \mathcal{X}} \pi_t(\mathbf{p}_t) \times \mathbf{C}(\mathbf{p}_t)$, in which $\pi_t(\mathbf{p}_t)$ is calculated using (10).
 - d) Channel estimation based on observations \mathcal{Y}_t :
 - i) $\mathbf{K}_t = \mathbf{Q}_{t|t-1} \mathbf{A}_t^H (\mathbf{A}_t \mathbf{Q}_{t|t-1} \mathbf{A}_t^H + \sigma_n^2 \mathbf{I})^{-1}$.
 - ii) $\hat{\mathbf{h}}_t = \hat{\mathbf{h}}_{t|t-1} + \mathbf{K}_t (\mathbf{y}_t - \mathbf{A}_t \hat{\mathbf{h}}_{t|t-1})$.
 - iii) $\mathbf{Q}_t = (\mathbf{I} - \mathbf{K}_t \mathbf{A}_t) \mathbf{Q}_{t|t-1}$.
 - e) Estimate the user position $\hat{\mathbf{p}}_t = \operatorname{argmax}_{\hat{\mathbf{p}}_t \in \mathcal{X}} p(\hat{\mathbf{h}}_t | \hat{\mathbf{h}}_{t|t-1}, \mathbf{p}_t) \mathbb{P}(\mathbf{p}_t | \hat{\mathbf{p}}_{t-1})$.
 - f) Output $\hat{\mathbf{h}}_t$ and $\hat{\mathbf{p}}_t$.

available, a random sensing matrix \mathbf{A}_t may be used. However, in the scenario of tracking, prior information is available for optimizing the sensing matrix \mathbf{A}_t for better CSI tracking. To achieve this, we investigate the differential entropy of $\hat{\mathbf{h}}_t$ with respect to (w.r.t.) \mathbf{A}_t .

1) *Differential Entropy*: First, to evaluate the uncertainty of the channel estimator $\hat{\mathbf{h}}_t$, we derive the differential entropy of $\hat{\mathbf{h}}_t$ w.r.t. the error covariance \mathbf{Q}_t .

From (18), the error covariance $\mathbb{E}\{(\mathbf{h}_t - \hat{\mathbf{h}}_t)(\mathbf{h}_t - \hat{\mathbf{h}}_t)^H\}$ of $\hat{\mathbf{h}}_t$ given the measurements \mathcal{Y}_t up to time t is captured in \mathbf{Q}_t , which implies that $\hat{\mathbf{h}}_t \sim \mathcal{CN}(\mathbf{h}_t, \mathbf{Q}_t)$. Following this, the differential entropy of $\hat{\mathbf{h}}_t$ is derived as [27, Theorem 8.4.1]

$$q(\hat{\mathbf{h}}_t) = \frac{N_t}{2} (1 + \log(2\pi)) + \frac{1}{2} \log |\mathbf{Q}_t|. \quad (23)$$

Similarly, based on (12) and (14), the differential entropy of $\hat{\mathbf{h}}_{t|t-1}$ is

$$q(\hat{\mathbf{h}}_{t|t-1}) = \frac{N_t}{2} (1 + \log(2\pi)) + \frac{1}{2} \log |\mathbf{Q}_{t|t-1}|. \quad (24)$$

Based on (23) and (24), we can express the differential entropy $q(\hat{\mathbf{h}}_t)$ given $q(\hat{\mathbf{h}}_{t|t-1})$ as

$$q(\hat{\mathbf{h}}_t) = q(\hat{\mathbf{h}}_{t|t-1}) + \frac{1}{2} (\log |\mathbf{Q}_t| - \log |\mathbf{Q}_{t|t-1}|). \quad (25)$$

Next, we minimize $q(\hat{\mathbf{h}}_t)$ w.r.t. the sensing matrix \mathbf{A}_t , which is embedded in \mathbf{Q}_t as indicated in (18). Given $q(\hat{\mathbf{h}}_{t|t-1})$ and (25), minimizing $q(\hat{\mathbf{h}}_t)$ is equivalent to minimizing $q(\hat{\mathbf{h}}_t) -$

$q(\hat{\mathbf{h}}_{t|t-1}) = \frac{1}{2}(\log |\mathbf{Q}_t| - \log |\mathbf{Q}_{t|t-1}|)$, which leads to the following optimization problem

$$\begin{aligned} & \underset{\mathbf{A}_t}{\text{minimize}} \quad \frac{1}{2}(\log |\mathbf{Q}_t| - \log |\mathbf{Q}_{t|t-1}|) \\ & \text{subject to} \quad \mathbf{A}_t \mathbf{A}_t^H = \mathbf{I}. \end{aligned} \quad (26)$$

2) *Solution for the Adaptive Sensing Matrix \mathbf{A}_t :* To solve Problem (26), we first explicitly derive the expression of $\frac{1}{2}(\log |\mathbf{Q}_t| - \log |\mathbf{Q}_{t|t-1}|)$ w.r.t. \mathbf{A}_t . Although we have derived $\mathbf{Q}_{t|t-1}$ and \mathbf{Q}_t in (14) and (18), it is not straightforward to derive $\frac{1}{2}(\log |\mathbf{Q}_t| - \log |\mathbf{Q}_{t|t-1}|)$ from them because \mathbf{Q}_t , $\mathbf{Q}_{t|t-1}$, \mathbf{Q}_{t-1} are recursively coupled. Thus, we provide the following proposition to offer an alternative *yet* equivalent transition from $\mathbf{Q}_{t|t-1}$ to \mathbf{Q}_t of (18).

Proposition 2 (Alternative error propagation process). *The error covariance \mathbf{Q}_t follows the following error propagation process*

$$\mathbf{Q}_t^{-1} = \mathbf{Q}_{t|t-1}^{-1} + \mathbf{A}_t^H (\sigma_n^2 \mathbf{I})^{-1} \mathbf{A}_t. \quad (27)$$

Proof. See Appendix B. \square

Taking the determinant of (27) yields

$$\begin{aligned} |\mathbf{Q}_t^{-1}| &= |\mathbf{Q}_{t|t-1}^{-1} + \mathbf{A}_t^H (\sigma_n^2 \mathbf{I})^{-1} \mathbf{A}_t| \\ &= |\mathbf{Q}_{t|t-1}^{-1}| |\mathbf{I} + \mathbf{Q}_{t|t-1}^{-1} \mathbf{A}_t^H (\sigma_n^2 \mathbf{I})^{-1} \mathbf{A}_t| \quad (28) \end{aligned}$$

$$= |\mathbf{Q}_{t|t-1}^{-1}| |\mathbf{I} + \sigma_n^{-2} \mathbf{A}_t \mathbf{Q}_{t|t-1}^{-1} \mathbf{A}_t^H|, \quad (29)$$

where equation (28) utilizes the multiplicative property of determinant, *i.e.*, $|\mathbf{XY}| = |\mathbf{X}||\mathbf{Y}|$, and equation (29) is based on the Weinstein-Aronszajn identity, *i.e.*, $|\mathbf{I}_m + \mathbf{XY}| = |\mathbf{I}_n + \mathbf{YX}|$.

Taking the logarithm of (29) and applying the inverse property of the determinant, we further have

$$\log |\mathbf{Q}_t| - \log |\mathbf{Q}_{t|t-1}| = -\log |\mathbf{I} + \sigma_n^{-2} \mathbf{A}_t \mathbf{Q}_{t|t-1}^{-1} \mathbf{A}_t^H|. \quad (30)$$

Thus, Problem (26) can be equivalently rewritten as

$$\begin{aligned} & \underset{\mathbf{A}_t}{\text{maximize}} \quad |\mathbf{I} + \sigma_n^{-2} \mathbf{A}_t \mathbf{Q}_{t|t-1}^{-1} \mathbf{A}_t^H| \\ & \text{subject to} \quad \mathbf{A}_t \mathbf{A}_t^H = \mathbf{I}. \end{aligned} \quad (31)$$

Problem (31) can be solved by utilizing eigenvalue decomposition (EVD) and properties of the determinant of a matrix as shown in the following proposition.

Proposition 3 (Adaptive sensing matrix). *The solution to problem (31) is given by*

$$\mathbf{A}_t = [\mathbf{w}_{t-1,1}, \mathbf{w}_{t-1,2}, \dots, \mathbf{w}_{t-1,m}, \dots, \mathbf{w}_{t-1,M}]^H, \quad (32)$$

where $\mathbf{w}_{t-1,m}$ is the eigenvector corresponding to the m th largest eigenvalue of the error covariance $\mathbf{Q}_{t|t-1}$.

Proof. See Appendix C. \square

Proposition 3 establishes a mechanism for adaptively adjusting sensing matrices \mathbf{A}_t by prioritizing subspaces with high information gain. To handle cases where the m th largest eigenvalue ($m \leq M$) exhibits multiplicity, resulting in a subspace spanned by multiple eigenvectors, one may use a randomization strategy to randomly select one eigenvector from this subspace.

In the initial stage, where prior information is scarce and $\mathbf{Q}_{t|t-1}$ approximates an identity matrix, the proposed strategy naturally degenerates to employing random sensing vectors, which is aligned with the strategies in the compressive sensing literature. As observations accumulate, guided by (23) and (30), the strategy progressively refines \mathbf{A}_t to minimize $\log |\mathbf{Q}_t|$, thereby adaptively sweeping through the subspace $\mathbf{Q}_{t|t-1}$ of the channel and reducing the differential entropy $q(\hat{\mathbf{h}}_t)$. This aligns with the beam sweeping strategy in the literature.

The adaptive sensing matrices can be incorporated into the proposed radio-map-embedded SKF framework for efficient channel sensing. However, the design of \mathbf{A}_t relies on the error covariance $\mathbf{Q}_{t|t-1}$, which is based on the position distribution $\pi_t(\mathbf{p}_t)$ calculated using the measurement \mathbf{y}_t . To address this implementation issue, the transition probability $\mathbb{P}(\mathbf{p}_t|\mathbf{p}_{t-1})$ is treated as the prior position distribution before observing \mathbf{y}_t . Hence, the error covariance $\mathbf{Q}_{t|t-1}$ is first computed using $\mathbb{P}(\mathbf{p}_t|\mathbf{p}_{t-1})$, and then refined via $\pi_t(\mathbf{p}_t)$ as detailed in Step 2 of Algorithm 1.

It is worth noting that the additional computational cost of the proposed adaptive sensing approach is primarily due to the eigendecomposition of $\mathbf{Q}_{t|t-1}$ since the design of \mathbf{A}_t depends on the error covariance $\mathbf{Q}_{t|t-1}$, whose computation has already been accounted for in the CSI tracking complexity analysis in Section III-B. While the eigendecomposition for a full-rank matrix requires a complexity of $O(N_t^3)$, there exist efficient algorithms with a complexity of $O(N_t^2)$ for decomposing a low-rank matrix.

IV. RADIO MAP CONSTRUCTION

In this section, we construct the radio map \mathcal{M} via estimating the hidden position variables \mathbf{p}_t and the corresponding channel covariances $\mathbf{C}(\mathbf{p}_t)$ as formulated in \mathcal{P}_2 . Note that the construction discussed here is decoupled from the CSI tracking problem studied in Section III.

While \mathcal{P}_2 also recovers the channel \mathbf{h}_t and the position \mathbf{p}_t , it differs from the CSI tracking problem in Section III in the following aspects: First, as the ultimate goal of Section III is to estimate the channel \mathbf{h}_t , the accuracy of the hidden position \mathbf{p}_t is not essential. By contrast, \mathcal{P}_2 aims at recovering accurate positions \mathbf{p}_t for radio map construction. Second, in \mathcal{P}_2 , an off-line solution is acceptable, where one can accumulate a large amount of sequential data $\{\mathcal{Y}_T^{(k)}\}$ that probably comes from different users k from different routes to enhance the estimation of the position \mathbf{p}_t . To illustrate the principle, we simply consider there is one user in one route that accumulates a sufficient amount of measurements. Third, while the anchor information for \mathbf{p}_t comes from the radio map \mathcal{M} in Section III, we need some side information Θ to recover \mathbf{p}_t in \mathcal{P}_2 , because the radio map \mathcal{M} is a variable to be optimized.

In this paper, we assume that a very coarse location $\tilde{\mathbf{p}}_t$ can be obtained from the side information of the network topology Θ , such as the BS locations. There is active research on coarse localization based on the sparse channel measurements \mathbf{y}_t [28], [29], such as using the weighted centroid localization (WCL) algorithm. It has been demonstrated in [28] using real

data that a localization error of 22 meters can be achieved by measuring only the received signal strength (RSS) from the BSs. In general, a $20 \sim 60$ meter RSS-based localization error is reported in the literature [29].

While a localization error of 20 meters is still too rough for radio map construction, the fundamental question to be investigated in this section is: *Can the radio-map-embedded CSI model substantially enhance the localization performance from coarse locations $\tilde{\mathbf{p}}_t$?*

A. Memory-Assisted Trajectory Discovery

Assume that a very coarse position $\tilde{\mathbf{p}}_t$ is available at time slot t . Denoting $\tilde{\mathcal{P}}_T = (\tilde{\mathbf{p}}_1, \tilde{\mathbf{p}}_2, \dots, \tilde{\mathbf{p}}_T)$, we define an L_2 -norm value function as $f(\mathcal{Y}_T, \mathcal{P}_T; \Theta) = \sum_{t=1}^T \|\mathbf{p}_t - \tilde{\mathbf{p}}_t\|_2$. Note that how to fuse the coarse position $\tilde{\mathbf{p}}_t$ to \mathcal{P}_2 is not the focus here, and other specifications of the value function $f(\mathcal{Y}_T, \mathcal{P}_T; \Theta)$ may also work. Problem \mathcal{P}_2 can be rewritten as

$$\begin{aligned} \mathcal{P}'_2 : \quad & \underset{\mathcal{H}_T, \mathcal{P}_T, \mathcal{M}}{\text{maximize}} \quad \log p(\mathcal{Y}_T, \mathcal{H}_T, \mathcal{P}_T; \mathcal{M}) \\ & \quad - \mu \sum_{t=1}^T \|\mathbf{p}_t - \tilde{\mathbf{p}}_t\|_2 \\ \text{subject to} \quad & \mathbf{p}_t \in \mathcal{X}, \quad t = 1, 2, \dots, T \end{aligned}$$

where $\mu > 0$ serves as a regularization parameter.

Since the observation \mathbf{y}_t depends on the hidden user position \mathbf{p}_t and the transition probability of \mathbf{p}_t is depicted by a mobility model (3), we can formulate an HMM problem with a regularization term for tracking the sequential states evolution of \mathcal{Y}_T and \mathcal{P}_T . Specifically, from the observation model (5), since \mathbf{y}_t depends on \mathbf{h}_t which depends on \mathbf{p}_t , we can marginalize \mathbf{h}_t from $p(\mathcal{Y}_T, \mathcal{H}_T, \mathcal{P}_T; \mathcal{M})$ to obtain

$$p(\mathcal{Y}_T, \mathcal{P}_T; \mathcal{M}) = \prod_{t=1}^T p(\mathbf{y}_t | \mathbf{p}_t; \mathcal{M}) \times \prod_{t=2}^T \mathbb{P}(\mathbf{p}_t | \mathbf{p}_{t-1}) \mathbb{P}(\mathbf{p}_1) \quad (33)$$

which follows the same derivation as that in (10).

Consequently, based on Problem \mathcal{P}'_2 , an HMM problem with a regularization term is formulated as

$$\begin{aligned} & \underset{\mathcal{P}_T}{\text{maximize}} \quad \sum_{t=1}^T (\log p(\mathbf{y}_t | \mathbf{p}_t; \mathcal{M}) + \mu \|\mathbf{p}_t - \tilde{\mathbf{p}}_t\|_2) \\ & \quad + \sum_{t=2}^T \log \mathbb{P}(\mathbf{p}_t | \mathbf{p}_{t-1}) + \log \mathbb{P}(\mathbf{p}_1) \quad (34) \end{aligned}$$

subject to $\mathbf{p}_t \in \mathcal{X}, \quad t = 1, 2, \dots, T$.

As indicated in (34), the trajectory discovery problem can be framed as an HMM decoding task, where the objective is to find the most likely sequence of hidden states (locations) that maximizes the regularized log-likelihood. Specifically, the log-likelihood $\log p(\mathbf{y}_t | \mathbf{p}_t; \mathcal{M}) + \log \mathbb{P}(\mathbf{p}_t | \mathbf{p}_{t-1})$ captures the hidden dynamics of the trajectory \mathcal{P}_T , while the regularization term $\mu \|\mathbf{p}_t - \tilde{\mathbf{p}}_t\|_2$ is to calibrate the topology \mathbf{p}_t with the geographic side information $\tilde{\mathbf{p}}_t$ from the physical world.

To solve Problem (34), the Viterbi algorithm can be employed to traverse all possible location sequences using dynamic programming to compute the optimal trajectory efficiently [30]. At each time step, the algorithm recursively evaluates the combined likelihood and transition probabilities of the best location sequence to a state \mathbf{p}_t , while incorporating the regularization term $\mu \|\mathbf{p}_t - \tilde{\mathbf{p}}_t\|_2$ to penalize deviations from $\tilde{\mathbf{p}}_t$. By maintaining backtracking pointers at each step, the algorithm tracks the location sequence with the highest accumulated objective value. This process ensures implicit exploration of all possible trajectories, with the most likely sequence retained as the final solution to Problem (34).

The time complexity for solving Problem (34) using the Viterbi algorithm is $O(T|\mathcal{X}|^2 N_t^3)$, where $O(T|\mathcal{X}|^2)$ is the time complexity of the Viterbi algorithm to handle a scalar variable transition process and $O(N_t^3)$ comes from the matrix inverse operation in $p(\mathbf{y}_t | \mathbf{p}_t)$ at each time step.

B. Covariance Estimation from Sparse CSI Measurements

Denote $\mathcal{T}_i \triangleq \{t : \mathbf{p}_t = \mathbf{x}_i \in \mathcal{X}\}$ as the set of measurements taken in the i th grid cell. We need to construct an estimator $\hat{\mathbf{C}}(\mathbf{x}_i)$ for the covariance matrix $\mathbf{C}(\mathbf{x}_i) = \mathbb{E}\{\mathbf{h}_t \mathbf{h}_t^H\} \in \mathbb{C}^{N_t \times N_t}$ based on the measurements $\mathbf{y}_t \in \mathbb{C}^M$, where $t \in \mathcal{T}_i$ and $M \ll N_t$. Assume that the measurements \mathbf{y}_t in the i th grid cell are independent. Otherwise, to ensure independence, a random subset of data can be sampled from the collected dataset. While we assume that there are a sufficient number of measurements that have been collected for discretized locations \mathbf{x}_i , it is still a challenge that the measurement \mathbf{y}_t has a very low dimension M .

1) *Unbiased Estimator of the Covariance*: The general idea is to construct a data point in the N_t -dimensional subspace spanned by the sensing matrix \mathbf{A}_t , and thus, the data point is defined as

$$\boldsymbol{\varphi}_t = \mathbf{A}_t^H \mathbf{y}_t = \mathbf{A}_t^H \mathbf{A}_t \mathbf{h}_t + \mathbf{A}_t^H \mathbf{n}_t = \boldsymbol{\Phi}_t \mathbf{h}_t + \mathbf{A}_t^H \mathbf{n}_t, \quad (35)$$

where $\boldsymbol{\Phi}_t = \mathbf{A}_t^H \mathbf{A}_t \in \mathbb{C}^{N_t \times N_t}$.

We then construct a sample covariance matrix as follows

$$\begin{aligned} \hat{\mathbf{\Omega}}_y(\mathbf{x}_i) & \triangleq \frac{N_t^2}{M^2} \frac{1}{|\mathcal{T}_i|} \sum_{t \in \mathcal{T}_i} \boldsymbol{\varphi}_t \boldsymbol{\varphi}_t^H \\ & = \frac{N_t^2}{|\mathcal{T}_i| M^2} \sum_{t \in \mathcal{T}_i} (\boldsymbol{\Phi}_t \mathbf{h}_t + \mathbf{A}_t^H \mathbf{n}_t) (\boldsymbol{\Phi}_t \mathbf{h}_t + \mathbf{A}_t^H \mathbf{n}_t)^H \end{aligned} \quad (36)$$

It can be shown that an unbiased estimator for the covariance matrix $\mathbf{C}(\mathbf{x}_i)$ can be constructed from the sample covariance matrix $\hat{\mathbf{\Omega}}_y(\mathbf{x}_i)$ as shown in the following proposition.

Proposition 4 (Unbiased estimator). *Let $\mathbf{A}_t \in \mathbb{C}^{M \times N_t}$ be an orthonormal basis for an M -dimensional subspace drawn uniformly at random. An unbiased estimator for $\mathbf{C}(\mathbf{x}_i)$ is given by*

$$\begin{aligned} \hat{\mathbf{C}}(\mathbf{x}_i) & = \frac{M(\bar{N}_t \hat{\mathbf{\Omega}}_y(\mathbf{x}_i) - (N_t - M) \text{tr}(\hat{\mathbf{\Omega}}_y(\mathbf{x}_i)) \mathbf{I})}{N_t(N_t M + N_t - 2)} \\ & \quad - \frac{\sigma_n^2 (M \bar{N}_t \mathbf{\Omega}_A(\mathbf{x}_i) - N_t(N_t - M) \text{tr}(\mathbf{\Omega}_A(\mathbf{x}_i)) \mathbf{I})}{M(N_t M + N_t - 2)}, \end{aligned} \quad (37)$$

where $\bar{N}_t \triangleq (N_t + 2)(N_t - 1)$ and $\Omega_A(\mathbf{x}_i) \triangleq \frac{1}{|\mathcal{T}_i|} \sum_{t \in \mathcal{T}_i} \mathbf{A}_t^H \mathbf{A}_t$.

Proof. See Appendix D. \square

The unbiased estimator $\hat{\mathbf{C}}(\mathbf{x}_i)$ in Proposition 4 is composed of a scaled version of the sample covariance of the CSI measurements, with an additional correction term that accounts for the noise covariance. Consider the special case where $M = N_t$ and $\Phi_t = \mathbf{A}_t^H \mathbf{A}_t = \mathbf{I}$, the estimator simplifies to $\hat{\mathbf{C}}(\mathbf{x}_i) = \sum_{t \in \mathcal{T}_i} (\varphi_t \varphi_t^H - \sigma_n^2 \mathbf{I}) / |\mathcal{T}_i|$. Next, we can take the expectation of $\hat{\mathbf{C}}(\mathbf{x}_i)$ and obtain that $\mathbb{E}\{\hat{\mathbf{C}}(\mathbf{x}_i)\} = \mathbb{E}\{\sum_{t \in \mathcal{T}_i} ((\mathbf{h}_t + \mathbf{A}_t^H \mathbf{n}_t)(\mathbf{h}_t + \mathbf{A}_t^H \mathbf{n}_t)^H - \sigma_n^2 \mathbf{I}) / |\mathcal{T}_i|\} = \mathbf{C}(\mathbf{x}_i)$.

Additionally, it is observed from (37) that the environmental noise is rescaled by \mathbf{A}_t and subsequently removed. In high SNR scenarios where σ_n^2 is small, the first term (measurement term) in (37) dominates the channel covariance estimation while the second term (noise term) can be considered negligible.

2) *Upper Bound of Reconstruction Error:* Here, we present the reconstruction error of the channel covariance $\mathbf{C}(\mathbf{x}_i)$ w.r.t. the CSI dimension N_t , the observation dimension M , the number of observations $|\mathcal{T}_i|$, and the rank of the true channel covariance $\mathbf{C}(\mathbf{x}_i)$.

Consider the high SNR case, where $\sigma_n = 0$, and the observed CSI is simplified as $\mathbf{y}_t = \mathbf{A}_t \mathbf{h}_t$. Based on (37), the unbiased estimator $\hat{\mathbf{C}}(\mathbf{x}_i)$ in (37) simplifies to

$$\hat{\mathbf{C}}'(\mathbf{x}_i) = \frac{M(\bar{N}_t \hat{\Omega}_y(\mathbf{x}_i) - (N_t - M)\text{tr}(\hat{\Omega}_y(\mathbf{x}_i))\mathbf{I})}{N_t(N_t M + N_2 - 2)}. \quad (38)$$

The following proposition shows the spectral upper bound of the reconstruction error $\hat{\mathbf{C}}'(\mathbf{x}_i) - \mathbf{C}(\mathbf{x}_i)$.

Proposition 5 (Upper bound of the reconstruction error). *Assuming $\text{rank}(\mathbf{C}(\mathbf{x}_i)) \leq R$, there exists a universal constant $\kappa > 0$ such that for any $\zeta \in (0, 1)$, when $N_t \geq 2$ and $|\mathcal{T}_i| \geq N_t \log(1/\zeta)$, with probability at least $1 - \zeta$,*

$$\|\hat{\mathbf{C}}'(\mathbf{x}_i) - \mathbf{C}(\mathbf{x}_i)\|_2 \leq \frac{\kappa}{\sqrt{|\mathcal{T}_i|}} \|\mathbf{C}(\mathbf{x}_i)\|_2 (S_1 + S_2 + S_3), \quad (39)$$

where $S_1 = \frac{\sqrt{N_t R^2 \log^2(|\mathcal{T}_i| N_t / \zeta)}}{M}$, $S_2 = \sqrt{R \log(1/\zeta)}$, and $S_3 = \frac{\sqrt{N_t R \log^2(|\mathcal{T}_i| N_t / \zeta)}}{\sqrt{|\mathcal{T}_i|} M}$.

Proof. Since \mathbf{h}_t follows a Gaussian distribution $\mathcal{CN}(0, \mathbf{C}(\mathbf{x}_i))$ and $\hat{\mathbf{C}}'(\mathbf{x}_i)$ is an unbiased estimator given in (38), applying Corollary 1 (Gaussian Upper Bounds) and Corollary 2 in [31] to our case automatically yields the results. \square

Proposition 5 provides key insights into the factors influencing the reconstruction error of sample covariance. First, if $|\mathcal{T}_i|$ is large relative to N_t^2/M^2 and the logarithmic factors are ignored, the leading terms in the error bound (39) is $\tilde{\mathcal{O}}(\|\mathbf{C}(\mathbf{x}_i)\|_2 (\sqrt{N_t R^2 / (|\mathcal{T}_i| M^2)} + N_t R / (|\mathcal{T}_i| M)))$, where the notation $\tilde{\mathcal{O}}(n)$ represents the asymptotic growth rate of a function n while suppressing dependencies on logarithmic factors. Thus, increasing the number of observation samples reduces error terms inversely, making it crucial to accumulate sufficient samples. Second, the upper bound in (39) decreases

inversely with M , and thus, increasing M may result in a reduction of the reconstruction error. Additionally, the rank of the true channel covariance highlights the difficulty of estimating channel covariance in NLOS environments with rich multipath effects. By contrast, in LOS environments, where R is small, reconstruction accuracy improves naturally, requiring fewer pilot signals (see Table. IV).

C. An Iterative Framework for Radio Map Construction

To sum up, a radio map construction framework is developed as follows. We begin with a sequence of sparse CSI measurements and apply the Viterbi algorithm to solve the user trajectory discovery problem (34). Based on the resulting user position estimates, the sparse CSI measurements are then assigned to the corresponding grid cells. Subsequently, we employ the unbiased estimator $\hat{\mathbf{C}}(\mathbf{x}_i)$ as defined in (37) to reconstruct the channel covariance $\mathbf{C}(\mathbf{x}_i)$ in each grid cell. This process yields the radio map \mathcal{M} , which is then used to perform a second round of trajectory discovery. Such a process is repeated until the change in estimated user positions between two iterations falls below a predefined threshold ϵ , at which point the radio map \mathcal{M} is considered finalized. Note that the trajectory discovery problem (34) requires an initialization of the channel covariance $\mathbf{C}(\mathbf{p}_t)$ to calculate $p(\mathbf{y}_t | \mathbf{p}_t)$. One can simply initialize identical channel covariance matrices for each discretized grid cell since $p(\mathbf{y}_t | \mathbf{p}_t)$ is only utilized for capturing relative relationships of user positions. The technical details are shown in Algorithm 2.

The iterative framework for radio map construction converges naturally as the trajectory and covariance estimates are progressively refined. In each iteration, the updated trajectory helps allocate CSI measurements to grid cells, improving the accuracy of the channel covariance matrices. These refined covariances then aid in discovering more accurate trajectories in the next iteration. This feedback loop stabilizes as changes in the estimated user positions decrease, eventually meeting the predefined threshold ϵ . While a formal proof of convergence is beyond this discussion, numerical results in Section V confirm the practical convergence of the framework (see Fig. 8).

Algorithm 2 Radio Map Construction

Input: The sparse CSI measurements \mathcal{Y}_T , coarse positions $\tilde{\mathcal{P}}_T$, the noise variance σ_n^2 , and a threshold ϵ .

- 1) Initialize $\mathcal{M}^{(l)} = \{(\mathbf{x}, \mathbf{I}) : \mathbf{x} \in \mathcal{X}\}$ and $\hat{\mathcal{P}}_T^{(l)} = \tilde{\mathcal{P}}_T$ at the iteration $l = 0$.
- 2) Repeat the following process until $\frac{1}{T} \sum_{t=1}^T \|\mathbf{p}_t^{(l)} - \mathbf{p}_t^{(l-1)}\|_2 < \epsilon$:
 - a) Set $l \leftarrow l + 1$.
 - b) Estimate the user trajectory $\hat{\mathcal{P}}_T^{(l)} = \{\hat{\mathbf{p}}_1^{(l)}, \hat{\mathbf{p}}_2^{(l)}, \dots, \hat{\mathbf{p}}_T^{(l)}\}$ by solving Problem (34).
 - c) Estimate the channel covariance $\hat{\mathbf{C}}^{(l)}(\mathbf{x}_i)$ using \mathcal{Y}_T , $\hat{\mathcal{P}}_T^{(l)}$, and (37), and construct the radio map $\hat{\mathcal{M}}^{(l)} = \{(\mathbf{x}, \hat{\mathbf{C}}^{(l)}(\mathbf{x})) : \mathbf{x} \in \mathcal{X}\}$.
- 3) Output $\hat{\mathcal{M}}^{(l)}$ and $\hat{\mathcal{P}}_T^{(l)}$.

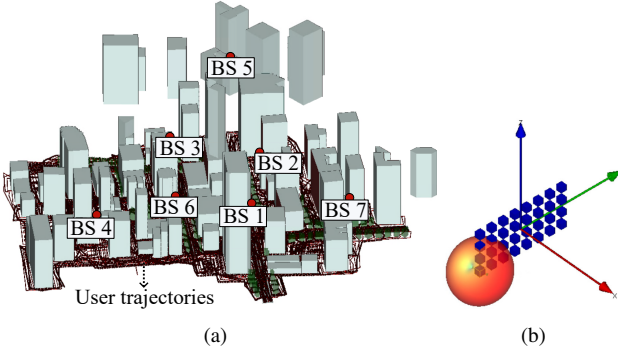


Figure 4. (a) Simulation environment with 7 BSs; (b) MIMO antenna with 32 dual-polarized dipole antenna arrays ($N_t = 64$).

V. NUMERICAL RESULTS

In this section, we present experimental findings on real-world city maps with 3D ray-traced MIMO channel datasets.

A. Environment Setup and Scenarios

The experiments are conducted on a MIMO CSI database generated by Wireless Insite¹ which provides 3D ray-tracing for the analysis of site-specific radio wave propagation. The tested city topology is a 710-meter \times 740-meter area from San Francisco, America. Seven BSs are deployed on the top of some buildings as shown in Fig. 4(a). The MIMO antenna of each BS consists of $N_t = 64$ antenna arrays as shown in Fig. 4(b). By simulating random walks along roads in the map, the radio database is established, and it contains 19331 user locations with 19331×7 MIMO channels.

The tested user trajectories are randomly generated along the road. The measurement $\mathbf{y}_t^{(q)}$ for the q th BS at the position \mathbf{p}_t is generated using (5), where the noise variance σ_n^2 is generated using the mean power of channels and the given SNR, *i.e.*, $\sigma_n^2 = \mathbb{E}\{\|\mathbf{h}_t^{(q)}\|_2^2\}/10^{\text{SNR}/10}$. Coarse user positions $\tilde{\mathbf{p}}_t$ are generated by adding a Gaussian random shift $\mathcal{N}(0, 900)$ to the true position \mathbf{p}_t . The radio map grid has a resolution of 5 meters, with the user moving at 10 meters/second and observations sampled every 10 milliseconds. The threshold ϵ for position change in Algorithm 2 is set to 0.5 meter. The dimension M of $\mathbf{y}_t^{(q)}$ is set to 1 for the proposed scheme.

Note that Doppler shift considerations are not necessary in our experimental setup. This is because the primary purpose of CSI estimation in the proposed scheme is to enable MIMO beamforming at the BS. Specifically, it aims to find a beamforming vector \mathbf{b} that maximizes the signal strength $|\mathbf{b}^H \mathbf{h} e^{-j\theta}|$, where the phase offset θ due to the Doppler effect does not affect the signal strength. During beamformed data transmission, additional pilot symbols are still required to compensate the phase offset θ . However, this aspect is beyond the scope of this work, which centers on reducing pilot overhead for CSI tracking to enable effective beamforming in mobile scenarios.

B. Baseline Schemes

The following baseline schemes are compared with the proposed CSI tracking scheme.

- Genius-aided CSI estimation: This scheme performs the proposed radio-map-embedded CSI tracking algorithm with known user positions and perfect radio maps.
- CAM-aided CSI estimation with one-shot measurement [20]: This scheme constructs a CAM to map locations to path gain magnitudes at known angles. The CAM serves as a localization fingerprint. $M = N_t/2$ beam vectors are designed based on the estimated AOD from the CAM for channel sensing, with the least squares (LS) method for channel estimation.
- AR-based CSI prediction [8]: This approach estimates AR coefficients of the channel based on the Yule-Walker equations and estimates the channel \mathbf{h}_t using 10 past channel estimates. The LS method is used for initial channel estimation with randomly generated $\mathbf{A}_t \in \mathbb{C}^{N_t \times N_t}$.
- LSTM-based CSI prediction [10]: This method adopts a recurrent neural network (RNN) and uses the previous 10 estimated channels to predict \mathbf{h}_t . Other settings are the same as those of the AR-based method.
- KF-based CSI tracking [26]: This scheme performs CSI tracking using KF with $M = 1$, and no radio map is used.
- LS-based CSI estimation: An LS estimate is given by $\hat{\mathbf{h}} = \mathbf{A}_t^\dagger \mathbf{y}$. Note that since we typically have $M < N_t$, we need to perform pseudo-inverse for the matrix \mathbf{A}_t . The sensing matrix \mathbf{A}_t is randomly generated with $M = N_t/2$.

The following metrics are used to evaluate the proposed algorithms: 1) Localization error: Given the true user position \mathbf{p}_t and the estimated user position $\hat{\mathbf{p}}_t$, the localization error is defined as $\frac{1}{T} \sum_{t=1}^T \|\mathbf{p}_t - \hat{\mathbf{p}}_t\|_2$. 2) Channel capacity: Using the maximum ratio combining (MRC) scheme, the channel capacity is expressed as $f(\mathbf{b}, \mathbf{h}) = \log_2(1 + |\mathbf{b}^H \mathbf{h}|^2/\sigma_n^2)$, where \mathbf{h} is the true CSI and $\mathbf{b} = \hat{\mathbf{h}}/\|\hat{\mathbf{h}}\|_2$ is the beamforming vector, in which $\hat{\mathbf{h}}$ is the estimated CSI. 3) Channel capacity efficiency ratio: This is defined as the ratio of the maximum capacity achieved with $\hat{\mathbf{h}}$ relative to that with perfect CSI \mathbf{h} . 4) Normalized L_2 -norm estimation error of channel covariance: This is defined as $\frac{1}{|\mathcal{X}|} \sum_{\mathbf{x} \in \mathcal{X}} \|\hat{\mathbf{C}}(\mathbf{x}) - \mathbf{C}(\mathbf{x})\|_2/\|\mathbf{C}(\mathbf{x})\|_2$.

C. Radio-Map-Embedded CSI Tracking

We first evaluate the proposed radio-map-embedded CSI tracking scheme. A perfect radio map \mathcal{M} for each BS is constructed by discretizing the area of interest and calculating $\mathbf{C}(\mathbf{x}_i)$ using true channels in each grid cell centered at \mathbf{x}_i . Fig. 5 illustrates the CSI and user position tracking performance of Algorithm 1. Specifically, Fig. 5(a) shows the channel capacity along a trajectory transitioning through NLOS, LOS, and NLOS regions to BS 7. The proposed scheme outperforms other baseline schemes, ensuring smooth tracking during the NLOS-LOS transition. Fig. 5(b) reveals that the channel capacity efficiency ratio of the proposed scheme remains above 90% for an LOS trajectory to BS 1. The tracking performance of the conventional KF scheme is

¹<http://www.remcom.com/wireless-insite>.

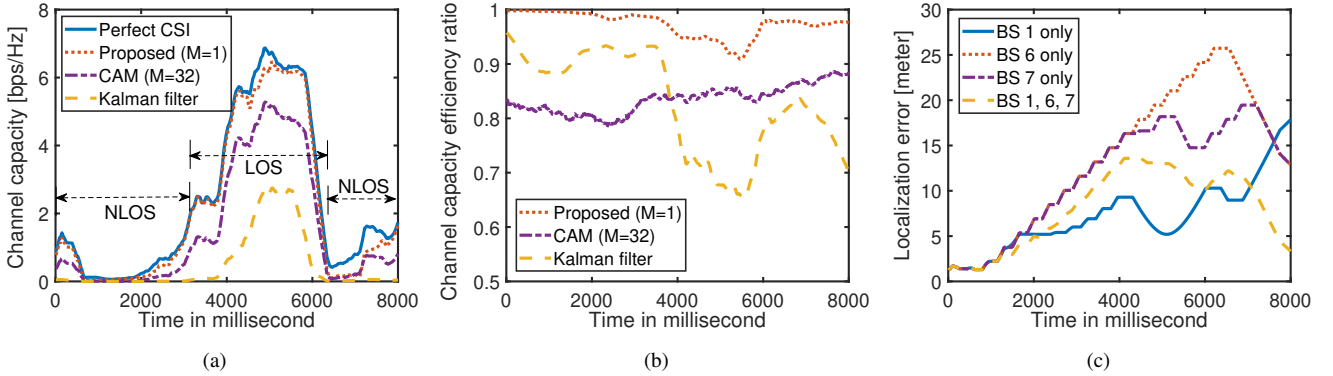


Figure 5. CSI and user position tracking performance. (a) Channel capacity for a trajectory transitioning through NLOS, LOS, and NLOS propagation conditions to BS 7; (b) Channel capacity efficiency ratio for an LOS trajectory to BS 1; (c) Localization error of the proposed radio-map-embedded CSI tracking scheme for the same trajectory in (a), which is LOS to BS 1 and NLOS to BS 6.

unstable due to the lack of prior CSI statistics, while the CAM-aided scheme achieves above 78% of capacity over that of perfect CSI. Fig. 5(c) highlights that localization errors along the same trajectory in Fig. 5(a) stay below 26 meters, where BS 1 operates under LOS conditions and BS 6 under NLOS. Additionally, the presence of multiple BSs contributes to more stable performance and reduced localization errors, with values consistently below 14 meters. For multi-BS cooperation, each BS independently computes the position distribution using (21), and then, these distributions are combined multiplicatively across BSs to form a joint posterior. Subsequently, the position $\mathbf{p}_t \in \mathcal{X}$ that maximizes this posterior is selected according to (22).

Fig. 6 shows the channel capacity efficiency ratio versus SNR when 7 BSs serve the user. This is merely an illustrative example to demonstrate the potential performance gains achievable with multiple BSs. The proposed scheme achieves over 97% of the capacity attained with perfect CSI at an SNR of 20 dB. Additionally, the proposed scheme nearly matches the performance of the genius-aided scheme, which assumes perfect user positions. The one-shot CAM scheme, which utilizes only the current measurement and 32 pilots ($M = 32$), achieves approximately 87% of the ideal capacity at an SNR of 30 dB. The KF scheme performs well at high SNR but achieves only about 36% of the ideal capacity at an SNR of 10 dB. The AR-based and LSTM-based methods perform poorly due to their dependence on highly accurate historical channel data and restrictive assumptions about stationary spatial distributions. The LS estimator consistently underperforms other baselines, because it fails to exploit spatial and temporal priors and relies solely on a one-shot observation for CSI estimation.

Fig. 7 depicts the channel capacity efficiency ratio versus BS groups under a 30 dB SNR. The randomly generated user trajectories are LOS to BSs 1 and 2 while they are NLOS to BSs 4 and 6. The proposed scheme achieves similar performance to the genius-aided scheme. Although some baseline schemes achieve over 83% of the ideal capacity in LOS cases, their performance degrades significantly in NLOS cases due to the highly complex CSI distributions caused by intricate urban topologies.

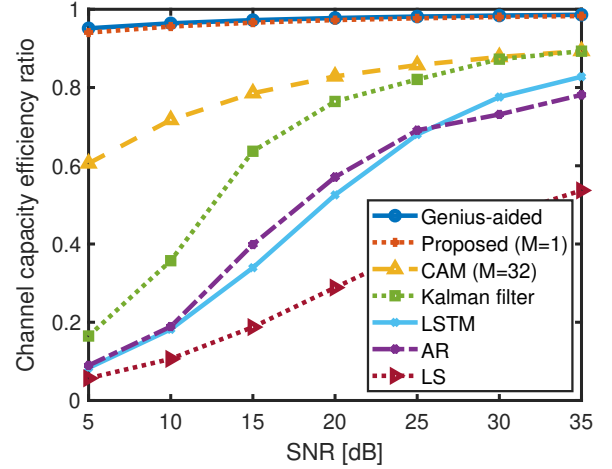


Figure 6. Channel capacity efficiency ratio versus SNR

Table I shows the impact of adaptive sensing matrices in the proposed CSI tracking scheme. It is observed that adaptive sensing provides additional performance gains, especially in low-SNR scenarios. For example, at 10 dB SNR under NLOS conditions to BS 6, the proposed method with adaptive \mathbf{A}_t achieves a channel capacity efficiency ratio of 55%, representing a 14% improvement over the same scheme with random \mathbf{A}_t . In addition, both variants of the proposed scheme with adaptive and random \mathbf{A}_t achieves over 91% of the ideal capacity under LOS conditions to BS 1, demonstrating the robustness of the proposed radio-map-embedded CSI tracking scheme, thanks to the strong spatial prior provided by the radio map.

Table II indicates that the coefficient γ in the channel model (4) has a negligible impact on the CSI tracking performance of the proposed scheme if it is within a certain range, e.g., [0.1, 0.7]. Moreover, the proposed scheme demonstrates stable and robust performance across a user speed range of 5 to 25 meters per second.

Additionally, Table III reports the average CSI estimation time at BS 1 under the same settings as Fig. 7. The proposed scheme takes approximately 0.27 ms to track the CSI for

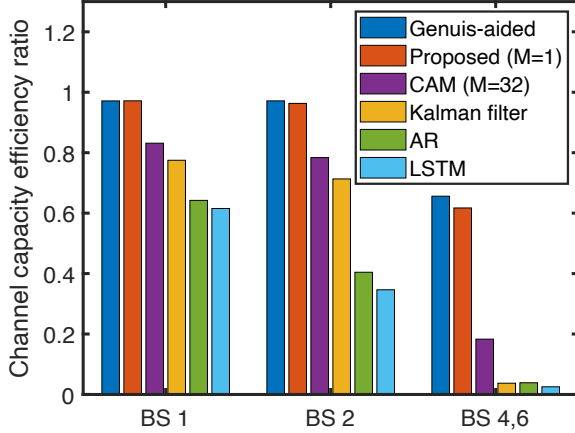


Figure 7. Channel capacity efficiency ratio versus BS groups

Table I

CHANNEL CAPACITY EFFICIENCY RATIO VERSUS SNR, WITH AND WITHOUT ADAPTIVE SENSING IN THE PROPOSED CSI TRACKING SCHEME

SNR [dB]	10	15	20	25	30
Adaptive sensing	BS 1	92%	93%	95%	97%
	BS 6	55%	55%	58%	58%
Random sensing	BS 1	91%	93%	95%	96%
	BS 6	41%	48%	50%	50%

BS 1, which is comparable to the CAM-aided scheme that achieves a similar running time of 0.27 ms but with a slightly lower channel capacity efficiency ratio of 83%. In contrast, schemes such as the KF-based and AR-based approaches are slightly faster (about 0.19 ms and 0.036 ms, respectively) but suffer from significant performance degradation, with over 21% lower capacity efficiency ratios.

D. Radio Map Construction

In this subsection, we construct radio maps for each BS from sparse and unlabeled pilot sequences in an offline manner. This is a one-time process performed prior to deployment. Fig. 8(a) shows an example of the estimated user trajectory obtained by solving Problem (34). The estimated trajectory matches the ground truth well, even though the coarse user locations are scattered over an area hundreds of meters wide. Numerical results indicate a localization error of less than

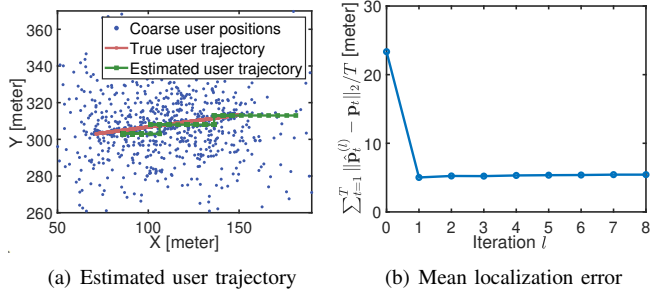


Figure 8. User localization and convergence of Algorithm 2.

Table IV
NORMALIZED L_2 -NORM ESTIMATION ERROR OF CHANNEL COVARIANCE VERSUS NUMBER OF MEASUREMENTS T_{total} AND DIMENSION M

T_{total}	35000	70000	105000	140000	175000
$M = 1$, BS 1 (LOS)	0.837	0.825	0.819	0.812	0.806
$M = 4$, BS 1 (LOS)	0.766	0.729	0.706	0.691	0.676
$M = 16$, BS 1 (LOS)	0.630	0.617	0.614	0.615	0.612
$M = 16$, BS 6 (NLOS)	0.781	0.762	0.755	0.748	0.742

6 meters when BS 1 serves the user. Fig. 8(b) confirms the convergence of Algorithm 2 with localization errors staying stable as the number of iterations increases.

Table IV presents the normalized L_2 -norm estimation error of the channel covariance versus the number of measurements T_{total} under different settings of M . Here, multiple sequences of channel measurements are collected, where each sequence consists of 350 measurements, and T_{total} denotes the total number of measurements across all sequences. Larger values of M and T_{total} reduce the normalized L_2 -norm estimation error as supported by Proposition 5. It is observed that when M is significantly smaller than N_t , e.g., $M = 4$, it requires 175,000 measurements to reach an estimation error of 0.676, while it only requires less than 35,000 measurements to achieve a smaller estimation error when $M = 16$. Additionally, constructing radio maps for BSs under NLOS conditions is more challenging compared to BSs under LOS due to the rich multipath effects.

Fig. 9 and Fig. 10 illustrate the CSI tracking performance for BS 1 under LOS conditions and BS 6 under NLOS, based on the radio maps that are reconstructed using 280,000 and 420,000 CSI measurements, respectively with $M = 16$. Using reconstructed radio maps, the proposed CSI tracking scheme with one pilot at each time slot and a total number of 100 pilots achieves above 88% of the ideal capacity for BS 1, and the proposed scheme outperforms other baseline schemes in both low-SNR and high-SNR scenarios for BS 6.

Additionally, the memory usage of the proposed radio map is assessed. The radio map covers an area of 740 m \times 710 m with a grid resolution of 5 m, resulting in 21,016 grids. Each grid stores its center coordinates as double-precision values and a 64×64 complex covariance matrix in single precision. The theoretical storage requirement is approximately 657 MB, and the actual uncompressed size is about 659 MB. This demonstrates the feasibility of the proposed method, as it

Table II

TRACK PERFORMANCE VERSUS γ ($\bar{v} = 10$) AND USER SPEED \bar{v} ($\gamma = 0.1$)

	$\gamma = 0.1$	$\gamma = 0.7$	$\bar{v} = 5$	$\bar{v} = 25$
Channel capacity efficiency ratio	98.0%	97.9%	98.7%	97.7%

Table III

AVERAGE RUNNING TIME FOR CSI ESTIMATION [MILLISECOND]

Genius	Proposed	CAM	KF	AR	LSTM
0.21	0.27	0.27	0.19	0.036	1.6

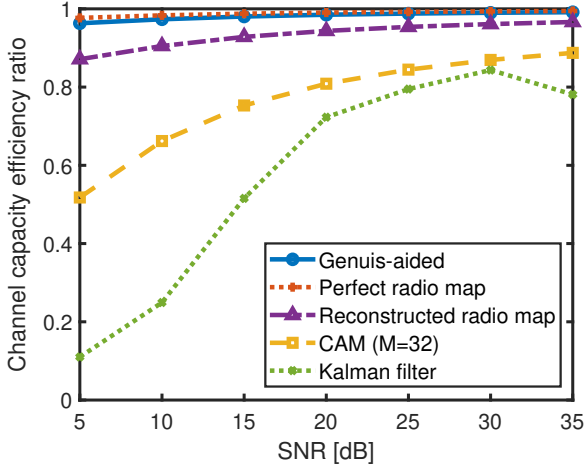


Figure 9. Channel capacity efficiency ratio for LOS trajectories to BS 1

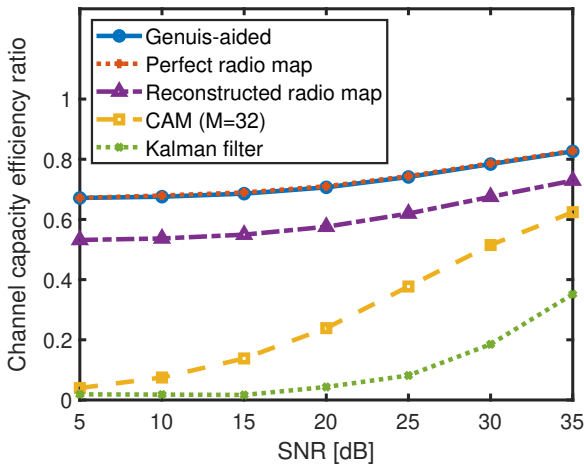


Figure 10. Channel capacity efficiency ratio for NLOS trajectories to BS 6

achieves a reasonable memory size while maintaining the necessary precision for the radio map.

VI. CONCLUSION

This paper addresses the challenges of CSI tracking in massive MIMO systems, particularly in the absence of stationary CSI statistics and precise location information. By integrating radio maps with an adaptive SKF framework, we track the CSI and the location using an extremely sparse pilot sequence without location labels. For radio map construction, the joint estimation of location sequences and channel covariance matrices is facilitated by an HMM, and an unbiased channel covariance estimator is found with the estimation error analyzed. Numerical results show that the proposed radio-map-embedded CSI tracking scheme delivers over 97% of the capacity of perfect CSI with reduced pilots at a 20 dB SNR under LOS, while a conventional KF can only achieve 76%. In addition, the proposed algorithm reduces localization errors from 30 meters from the prior to 6 meters for radio map construction in our framework.

APPENDIX A PROOF OF PROPOSITION 1

According to Bayes' theorem, $p(\mathcal{Y}_T, \mathcal{H}_T)$ is derived as

$$\begin{aligned} p(\mathcal{Y}_T, \mathcal{H}_T) &= p(\mathbf{y}_T | \mathcal{Y}_{T-1}, \mathcal{H}_T) p(\mathcal{Y}_{T-1}, \mathcal{H}_T) \\ &= p(\mathbf{y}_T | \mathbf{h}_T) P(\mathbf{h}_T | \mathcal{Y}_{T-1}, \mathcal{H}_{T-1}) p(\mathcal{Y}_{T-1}, \mathcal{H}_{T-1}) \end{aligned} \quad (40)$$

$$= p(\mathbf{y}_T | \mathbf{h}_T) P(\mathbf{h}_T | \mathbf{h}_{T-1}, \mathbf{p}_T) p(\mathcal{Y}_{T-1}, \mathcal{H}_{T-1}) \quad (41)$$

$$= \prod_{t=1}^T p(\mathbf{y}_t | \mathbf{h}_t) \times \prod_{t=2}^T p(\mathbf{h}_t | \mathbf{h}_{t-1}, \mathbf{p}_t) p(\mathbf{h}_1), \quad (42)$$

where equations (40) and (41) hold because \mathbf{y}_T depends on \mathbf{h}_T , and \mathbf{h}_T depends on \mathbf{h}_{T-1} and \mathbf{p}_T , and equation (42) is derived by recursively decomposing $p(\mathcal{Y}_{T-1}, \mathcal{H}_{T-1})$ in the same manner as $p(\mathcal{Y}_T, \mathcal{H}_T)$. Thus, $p(\mathcal{Y}_T | \mathcal{H}_T)$ is derived as

$$p(\mathcal{Y}_T | \mathcal{H}_T) = p(\mathcal{Y}_T, \mathcal{H}_T) / p(\mathcal{H}_T) = \prod_{t=1}^T p(\mathbf{y}_t | \mathbf{h}_t) \quad (43)$$

Similar to (42), $p(\mathcal{H}_T, \mathcal{P}_T)$ is derived as

$$p(\mathcal{H}_T, \mathcal{P}_T) = \prod_{t=2}^T p(\mathbf{h}_t | \mathbf{h}_{t-1}, \mathbf{p}_t) \mathbb{P}(\mathbf{p}_t | \mathbf{p}_{t-1}) p(\mathbf{h}_1) \mathbb{P}(\mathbf{p}_1). \quad (44)$$

Based on (43) and (44), $p(\mathcal{Y}_T, \mathcal{P}_T, \mathcal{H}_T)$ is factorized as

$$\begin{aligned} p(\mathcal{Y}_T, \mathcal{P}_T, \mathcal{H}_T) &= p(\mathcal{Y}_T | \mathcal{P}_T, \mathcal{H}_T) p(\mathcal{H}_T, \mathcal{P}_T) \\ &= p(\mathcal{Y}_T | \mathcal{H}_T) p(\mathcal{H}_T, \mathcal{P}_T) \end{aligned} \quad (45)$$

$$\begin{aligned} &= \prod_{t=1}^T p(\mathbf{y}_t | \mathbf{h}_t) \prod_{t=2}^T p(\mathbf{h}_t | \mathbf{h}_{t-1}, \mathbf{p}_t) p(\mathbf{h}_1) \\ &\quad \times \prod_{t=2}^T \mathbb{P}(\mathbf{p}_t | \mathbf{p}_{t-1}) \mathbb{P}(\mathbf{p}_1), \end{aligned} \quad (46)$$

where (45) holds because \mathbf{y}_t is independent of \mathbf{p}_t given \mathbf{h}_t .

APPENDIX B PROOF OF PROPOSITION 2

The error propagation process can be proved by validating $\mathbf{Q}_t \mathbf{Q}_t^{-1} = \mathbf{I}$, where \mathbf{Q}_t is in (18) and \mathbf{Q}_t^{-1} is in (27).

First, substituting the optimal \mathbf{K}_t in (17) into (18), we have

$$\mathbf{Q}_t = \mathbf{Q}_{t|t-1} - \mathbf{Q}_{t|t-1} \mathbf{A}_t^H (\mathbf{A}_t \mathbf{Q}_{t|t-1} \mathbf{A}_t^H + \sigma_n^2 \mathbf{I})^{-1} \mathbf{A}_t \mathbf{Q}_{t|t-1}. \quad (47)$$

Second, $\mathbf{Q}_t \mathbf{Q}_t^{-1}$ is derived as

$$\begin{aligned} \mathbf{Q}_t \mathbf{Q}_t^{-1} &= (\mathbf{Q}_{t|t-1} - \mathbf{Q}_{t|t-1} \mathbf{A}_t^H (\mathbf{A}_t \mathbf{Q}_{t|t-1} \mathbf{A}_t^H + \sigma_n^2 \mathbf{I})^{-1} \mathbf{A}_t) \\ &\quad \times \mathbf{A}_t \mathbf{Q}_{t|t-1}) (\mathbf{Q}_{t|t-1}^{-1} + \mathbf{A}_t^H (\sigma_n^2 \mathbf{I})^{-1} \mathbf{A}_t) \\ &= \mathbf{I} - \mathbf{Q}_{t|t-1} \mathbf{A}_t^H [(\mathbf{A}_t \mathbf{Q}_{t|t-1} \mathbf{A}_t^H + \sigma_n^2 \mathbf{I})^{-1} - (\sigma_n^2 \mathbf{I})^{-1}] \\ &\quad + (\mathbf{A}_t \mathbf{Q}_{t|t-1} \mathbf{A}_t^H + \sigma_n^2 \mathbf{I})^{-1} \mathbf{A}_t \mathbf{Q}_{t|t-1} \mathbf{A}_t^H (\sigma_n^2 \mathbf{I})^{-1} \mathbf{A}_t \\ &= \mathbf{I} - \mathbf{Q}_{t|t-1} \mathbf{A}_t^H [(\sigma_n^2 \mathbf{I})^{-1} - (\sigma_n^2 \mathbf{I})^{-1}] \mathbf{A}_t \\ &= \mathbf{I}. \end{aligned}$$

Thus, \mathbf{Q}_t^{-1} in (27) is the inverse of \mathbf{Q}_t .

APPENDIX C PROOF OF PROPOSITION 3

Using EVD of $\mathbf{Q}_{t|t-1}$, we have

$$\mathbf{Q}_{t|t-1} = \mathbf{W}_{t-1} \mathbf{\Lambda}_{t-1} \mathbf{W}_{t-1}^H, \quad (48)$$

where $\mathbf{\Lambda}_{t-1} = \text{diag}\{\lambda_{t-1,1}, \dots, \lambda_{t-1,N_t}\}$ is a diagonal matrix containing the eigenvalues of $\mathbf{Q}_{t|t-1}$ in descending order and $\mathbf{W}_{t-1} = [\mathbf{w}_{t-1,1}, \mathbf{w}_{t-1,2}, \dots, \mathbf{w}_{t-1,N_t}]$ is a unitary matrix with orthogonal eigenvectors of $\mathbf{Q}_{t|t-1}$.

Define $\mathbf{B}_t \triangleq \mathbf{A}_t \mathbf{W}_{t-1} \in \mathbb{C}^{M \times N_t}$. Based on (48), $|\mathbf{I} + \sigma_n^{-2} \mathbf{A}_t \mathbf{Q}_{t|t-1} \mathbf{A}_t^H|$ is derived as

$$\begin{aligned} |\mathbf{I} + \sigma_n^{-2} \mathbf{A}_t \mathbf{Q}_{t|t-1} \mathbf{A}_t^H| &= |\mathbf{I} + \sigma_n^{-2} \mathbf{A}_t \mathbf{W}_{t-1} \mathbf{\Lambda}_{t-1} \mathbf{W}_{t-1}^H \mathbf{A}_t^H| \\ &= |\mathbf{I} + \sigma_n^{-2} \mathbf{B}_t \mathbf{\Lambda}_{t-1} \mathbf{B}_t^H| \\ &= |\mathbf{B}_t (\mathbf{I} + \sigma_n^{-2} \mathbf{\Lambda}_{t-1}) \mathbf{B}_t^H|. \end{aligned} \quad (49)$$

The matrix $\mathbf{B}_t (\mathbf{I} + \sigma_n^{-2} \mathbf{\Lambda}_{t-1}) \mathbf{B}_t^H$ is a projection of the diagonal matrix $\mathbf{I} + \sigma_n^{-2} \mathbf{\Lambda}_{t-1}$ onto the subspace defined by \mathbf{B}_t with $\mathbf{B}_t \mathbf{B}_t^H = \mathbf{A}_t \mathbf{W}_{t-1} (\mathbf{A}_t \mathbf{W}_{t-1})^H = \mathbf{I}$. To maximize $|\mathbf{B}_t (\mathbf{I} + \sigma_n^{-2} \mathbf{\Lambda}_{t-1}) \mathbf{B}_t^H|$, \mathbf{B}_t should select the top M eigenvalues of $\mathbf{I} + \sigma_n^{-2} \mathbf{\Lambda}_{t-1}$.

Thus, $|\mathbf{B}_t (\mathbf{I} + \sigma_n^{-2} \mathbf{\Lambda}_{t-1}) \mathbf{B}_t^H|$ reaches its maximum as $\prod_{i=1}^M (1 + \sigma_n^2 \lambda_{t-1,i})$, where $\lambda_{t-1,i}$ for $i = 1, 2, \dots, M$ are the top M eigenvalues of $\mathbf{Q}_{t|t-1}$. In this case, \mathbf{A}_t is given by $\mathbf{A}_t = [\mathbf{w}_{t-1,1}, \mathbf{w}_{t-1,2}, \dots, \mathbf{w}_{t-1,M}]^H$ such that $\mathbf{B}_t = \mathbf{A}_t \mathbf{W}_{t-1}$ is a diagonal matrix with its first M diagonal elements equal to 1 and other elements equal to 0.

APPENDIX D PROOF OF PROPOSITION 4

It suffices to consider $\mathcal{T}_i = \{1\}$ and $t = 1$ as the result will follow by linearity of expectation in each discretize region. Let $\mathbf{h} = \mathbf{h}_1$, $\Phi = \Phi_1$, $\mathbf{n} = \mathbf{n}_1$, and $\mathbf{A} = \mathbf{A}_1$.

First, $\mathbb{E}\{\hat{\Omega}_y(\mathbf{x}_i)|\mathbf{h}\}$ is expressed as

$$\begin{aligned} \mathbb{E}\{\hat{\Omega}_y(\mathbf{x}_i)|\mathbf{h}\} &= \frac{N_t^2}{M^2} \mathbb{E}\{(\Phi \mathbf{h} + \mathbf{A}^H \mathbf{n})(\Phi \mathbf{h} + \mathbf{A}^H \mathbf{n})^H | \mathbf{h}\} \\ &= \frac{N_t^2}{M^2} (\mathbb{E}\{\Phi \mathbf{h} (\Phi \mathbf{h})^H | \mathbf{h}\} + \mathbb{E}\{\mathbf{A}^H \mathbf{n} \mathbf{n}^H \mathbf{A}\}), \end{aligned}$$

where the cross terms are dropped because of the independence of the signal and the noise.

Second, the following fact is adopted from [31, Fact 1].

Fact 1. If $\mathbf{x} \in \mathbb{C}^{N_t}$ and $\Phi \in \mathbb{C}^{N_t \times N_t}$ is a uniformly distributed rank m orthogonal projection, then

$$\Phi \mathbf{x} \stackrel{d}{=} \omega \mathbf{x} + \sqrt{\omega - \omega^2} \|\mathbf{x}\| \mathbf{W} \mathbf{\Omega},$$

where $\omega \sim \text{Beta}(\frac{M}{2}, \frac{N_t - M}{2})$, $\mathbf{\Omega} \in \mathbb{C}^{N_t-1}$ is distributed uniformly on the unit sphere and independent from ω , and $\mathbf{W} \in \mathbb{C}^{N_t \times (N_t-1)}$ is an orthonormal basis for the subspace orthogonal to \mathbf{x} , i.e., $\mathbf{x}^H \mathbf{W} = 0$.

Based on Fact 1 and the expectation of Beta distribution, $\mathbb{E}\{\Phi \mathbf{h} (\Phi \mathbf{h})^H | \mathbf{h}\}$ can be derived and simplified as

$$\begin{aligned} \mathbb{E}\{\Phi \mathbf{h} (\Phi \mathbf{h})^H | \mathbf{h}\} &= \frac{M(MN_t + N_t - 2)\mathbf{h}\mathbf{h}^H}{N_t(N_t + 2)(N_t - 1)} \\ &\quad + \frac{M(N_t - M)\text{tr}(\mathbf{h}\mathbf{h}^H)\mathbf{I}}{N_t(N_t + 2)(N_t - 1)}. \end{aligned} \quad (50)$$

Third, since $\mathbf{n} \sim \mathcal{CN}(0, \sigma_n^2 \mathbf{I})$ and \mathbf{n} is independent of \mathbf{A} , the expectation $\mathbb{E}\{\mathbf{A}^H \mathbf{n} \mathbf{n}^H \mathbf{A}\}$ is derived as

$$\mathbb{E}\{\mathbf{A}^H \mathbf{n} \mathbf{n}^H \mathbf{A}\} = \mathbf{A}^H \mathbb{E}\{\mathbf{n} \mathbf{n}^H\} \mathbf{A} = \sigma_n^2 \mathbf{A}^H \mathbf{A}. \quad (51)$$

Fourth, by taking the expectation of $\mathbb{E}\{\hat{\Omega}_y(\mathbf{x}_i)|\mathbf{h}\}$ over \mathbf{h} and rescaling (50) and (51) by N_t^2/M^2 , $\mathbb{E}\{\hat{\Omega}_y(\mathbf{x}_i)\}$ is derived as

$$\begin{aligned} \mathbb{E}\{\hat{\Omega}_y(\mathbf{x}_i)\} &= \frac{N_t(MN_t + N_t - 2)}{M(N_t + 2)(N_t - 1)} \mathbf{C}(\mathbf{x}_i) \\ &\quad + \frac{N_t(N_t - M)\text{tr}(\mathbf{C}(\mathbf{x}_i))\mathbf{I}}{M(N_t + 2)(N_t - 1)} \\ &\quad + \frac{N_t^2 \sigma_n^2}{M^2 |\mathcal{T}_i|} \sum_{t \in \mathcal{T}_i} \mathbf{A}_t^H \mathbf{A}_t. \end{aligned} \quad (52)$$

Fifth, by taking the trace operation to both sides of (52), and extracting the term $\text{tr}(\mathbf{C}(\mathbf{x}_i))$, we have

$$\text{tr}(\mathbf{C}(\mathbf{x}_i)) = \frac{M}{N_t} \text{tr}(\mathbb{E}\{\hat{\Omega}_y(\mathbf{x}_i)\}) - \frac{N_t \sigma_n^2}{M |\mathcal{T}_i|} \sum_{t \in \mathcal{T}_i} \text{tr}(\mathbf{A}_t^H \mathbf{A}_t).$$

Substituting the above $\text{tr}(\mathbf{C}(\mathbf{x}_i))$ into (52), we can obtain

$$\begin{aligned} \mathbb{E}\{\hat{\Omega}_y(\mathbf{x}_i)\} &= \frac{N_t(MN_t + N_t - 2)}{M(N_t + 2)(N_t - 1)} \mathbf{C}(\mathbf{x}_i) \\ &\quad + \frac{(N_t - M)}{(N_t + 2)(N_t - 1)} \text{tr}(\mathbb{E}\{\hat{\Omega}_y(\mathbf{x}_i)\}) \mathbf{I} \\ &\quad - \frac{N_t^2(N_t - M)\sigma_n^2}{M^2(N_t + 2)(N_t - 1)|\mathcal{T}_i|} \sum_{t \in \mathcal{T}_i} \text{tr}(\mathbf{A}_t^H \mathbf{A}_t) \mathbf{I} \\ &\quad + \frac{N_t^2 \sigma_n^2}{M^2 |\mathcal{T}_i|} \sum_{t \in \mathcal{T}_i} \mathbf{A}_t^H \mathbf{A}_t. \end{aligned} \quad (53)$$

Finally, $\mathbf{C}(\mathbf{x}_i)$ can be extracted from (53) as

$$\begin{aligned} \mathbf{C}(\mathbf{x}_i) &= \frac{M(\bar{N}_t \mathbb{E}\{\hat{\Omega}_y(\mathbf{x}_i)\} - (N_t - M)\text{tr}(\mathbb{E}\{\hat{\Omega}_y(\mathbf{x}_i)\})\mathbf{I})}{N_t(N_t M + N_t - 2)} \\ &\quad - \frac{\sigma_n^2(M\bar{N}_t \mathbf{\Omega}_A(\mathbf{x}_i) - N_t(N_t - M)\text{tr}(\mathbf{\Omega}_A(\mathbf{x}_i))\mathbf{I})}{M(N_t M + N_t - 2)}, \end{aligned} \quad (54)$$

where $\bar{N}_t \triangleq N_t^2 + N_t - 2$ and $\mathbf{\Omega}_A(\mathbf{x}_i) \triangleq \frac{1}{|\mathcal{T}_i|} \sum_{t \in \mathcal{T}_i} \mathbf{A}_t^H \mathbf{A}_t$.

Since trace is a linear operator, we immediately see that our estimator $\hat{\mathbf{C}}(\mathbf{x}_i)$ in (37) is unbiased as $\mathbb{E}\{\hat{\mathbf{C}}(\mathbf{x}_i)\} = \mathbf{C}(\mathbf{x}_i)$.

REFERENCES

- [1] H. Guo and V. K. N. Lau, "Bayesian hierarchical sparse autoencoder for massive MIMO CSI feedback," *IEEE Trans. Signal Process.*, vol. 72, pp. 3213–3227, 2024.
- [2] Z. He, H. Shen, W. Xu, Y. C. Eldar, and X. You, "MSE-based training and transmission optimization for MIMO ISAC systems," *IEEE Trans. Signal Process.*, vol. 72, pp. 3104–3121, 2024.
- [3] L. V. Nguyen, A. L. Swindlehurst, and D. H. N. Nguyen, "Variational bayes for joint channel estimation and data detection in few-bit massive MIMO systems," *IEEE Trans. Signal Process.*, vol. 72, pp. 3408–3423, 2024.
- [4] A. Mehrotra, S. Srivastava, S. Asifa, A. K. Jagannatham, and L. Hanzo, "Online Bayesian learning-aided sparse CSI estimation in OTFS modulated MIMO systems for ultra-high-Doppler scenarios," *IEEE Trans. on Commun.*, vol. 72, no. 4, pp. 2182–2200, 2024.
- [5] M. Ke, Z. Gao, Y. Wu, X. Gao, and R. Schober, "Compressive sensing-based adaptive active user detection and channel estimation: Massive access meets massive MIMO," *IEEE Trans. Signal Process.*, vol. 68, pp. 764–779, 2020.

[6] Y. Wan, G. Liu, A. Liu, and M.-J. Zhao, "Robust multi-user channel tracking scheme for 5G new radio," *IEEE Trans. on Wireless Commun.*, vol. 23, no. 6, pp. 5878–5894, 2024.

[7] D. R. Brown, R. Wang, and S. Dasgupta, "Channel state tracking for large-scale distributed MIMO communication systems," *IEEE Trans. Signal Process.*, vol. 63, no. 10, pp. 2559–2571, 2015.

[8] J. Vinogradova, G. Fodor, and P. Hammarberg, "On estimating the autoregressive coefficients of time-varying fading channels," in *Proc. IEEE Veh. Technol. Conf. (VTC)*, pp. 1–5, Helsinki, Finland, 2022.

[9] Y. Zhao, X. Zhang, X. Gao, K. Yang, Z. Xiong, and Z. Han, "LSTM-based predictive mmwave beam tracking via sub-6 GHz channels for V2I communications," *IEEE Trans. on Commun.*, 2024, early access.

[10] T. Peng, R. Zhang, X. Cheng, and L. Yang, "LSTM-based channel prediction for secure massive MIMO communications under imperfect CSI," in *Proc. IEEE Int. Conf. Commun.*, pp. 1–6, Dublin, Ireland, 2020.

[11] B. Zhou, X. Yang, S. Ma, F. Gao, and G. Yang, "Pay less but get more: A dual-attention-based channel estimation network for massive MIMO systems with low-density pilots," *IEEE Trans. on Wireless Commun.*, vol. 23, no. 6, pp. 6061–6076, 2024.

[12] J. Mirzaei, S. Shahbaz Panahi, R. S. Adve, and N. K. M. Gopal, "Deep generative models for downlink channel estimation in FDD massive MIMO systems," *IEEE Trans. Signal Process.*, vol. 70, pp. 2000–2014, 2022.

[13] Y. Zeng, J. Chen, J. Xu, D. Wu, X. Xu, S. Jin, X. Gao, D. Gesbert, S. Cui, and R. Zhang, "A tutorial on environment-aware communications via channel knowledge map for 6G," *IEEE Commun. Surveys Tuts.*, vol. 26, no. 3, pp. 1478–1519, 2024.

[14] Y. Zheng, M. Jia, and J. Chen, "Discovering CSI evolution using radio map for massive MIMO channel estimation," in *Proc. IEEE Int. Conf. Commun.*, pp. 5117–5122, 2024.

[15] D. Wu, Y. Zeng, S. Jin, and R. Zhang, "Environment-aware hybrid beamforming by leveraging channel knowledge map," *IEEE Trans. on Wireless Commun.*, vol. 23, no. 5, pp. 4990–5005, 2024.

[16] H. Chung and S. Kim, "Location-aware beam training and multi-dimensional ANM-based channel estimation for RIS-aided mmwave systems," *IEEE Trans. on Wireless Commun.*, vol. 23, no. 1, pp. 652–666, 2024.

[17] Z. Yu, X. Hu, C. Liu, M. Peng, and C. Zhong, "Location sensing and beamforming design for IRS-enabled multi-user ISAC systems," *IEEE Trans. Signal Process.*, vol. 70, pp. 5178–5193, 2022.

[18] J. Du, Y. Cheng, L. Jin, S. Li, and F. Gao, "Nested tensor-based integrated sensing and communication in RIS-assisted thz MIMO systems," *IEEE Trans. Signal Process.*, vol. 72, pp. 1141–1157, 2024.

[19] Z. Dai, D. Wu, Z. Dong, K. Li, D. Ding, S. Wang, and Y. Zeng, "Prototyping and experimental results for environment-aware millimeter wave beam alignment via channel knowledge map," *IEEE Trans. Veh. Technol.*, vol. 73, no. 11, pp. 16 805–16 816, 2024.

[20] D. Wu and Y. Zeng, "Environment-aware coordinated multi-point mmwave beam alignment via channel knowledge map," in *Proc. IEEE Int. Conf. Commun. Workshop*, pp. 1044–1049, Rome, Italy, 2023.

[21] M. Stahlke, G. Yammie, T. Feigl, B. M. Eskofier, and C. Mutschler, "Velocity-based channel charting with spatial distribution map matching," *IEEE J. Indoor Seamless Position Navig.*, vol. 2, pp. 230–239, 2024.

[22] P. Ferrand, M. Guillaud, C. Studer, and O. Tirkkonen, "Wireless channel charting: Theory, practice, and applications," *IEEE Commun. Mag.*, vol. 61, no. 6, pp. 124–130, 2023.

[23] G. Zhou, C. Pan, H. Ren, P. Popovski, and A. L. Swindlehurst, "Channel estimation for RIS-aided multiuser millimeter-wave systems," *IEEE Trans. Signal Process.*, vol. 70, pp. 1478–1492, 2022.

[24] B. Liang and Z. Haas, "Predictive distance-based mobility management for PCS networks," in *Proc. IEEE INFOCOM*, vol. 3, 1999, pp. 1377–1384.

[25] J. Wang, Q. Zhu, Z. Lin, J. Chen, G. Ding, Q. Wu, G. Gu, and Q. Gao, "Sparse bayesian learning-based hierarchical construction for 3D radio environment maps incorporating channel shadowing," *IEEE Trans. on Wireless Commun.*, vol. 23, no. 10, pp. 14 560–14 574, 2024.

[26] G. Welch and G. Bishop, *An Introduction to the Kalman Filter*. Chapel Hill, NC, USA: University of North Carolina at Chapel Hill, 1995.

[27] T. M. and J. A. Thomas, *Elements of Information Theory (Wiley Series in Telecommunications and Signal Processing)*. USA: Wiley-Interscience, 2006.

[28] Z. Xing and J. Chen, "Constructing indoor region-based radio map without location labels," *IEEE Trans. Signal Process.*, vol. 72, pp. 2512–2526, 2024.

[29] K. Magowe, A. Giorgetti, S. Kandeepan, and X. Yu, "Accurate analysis of weighted centroid localization," *IEEE Trans. on Cognitive Commun. and Networking*, vol. 5, no. 1, pp. 153–164, 2018.

[30] W. H. Press, S. A. Teukolsky, W. T. Vetterling, and B. P. Flannery, *Numerical Recipes 3rd Edition: The Art of Scientific Computing*, 3rd ed. USA: Cambridge University Press, 2007.

[31] M. Azizyan, A. Krishnamurthy, and A. Singh, "Extreme compressive sampling for covariance estimation," *IEEE Trans. Inf. Theory*, vol. 64, no. 12, pp. 7613–7635, 2018.